Proton-Sensitive Transitions of Renal Type II Na^+-Coupled Phosphate Cotransporter Kinetics

Ian C. Forster, Jürg Biber, and Heini Murer
Institute of Physiology, University of Zurich, Zurich, Switzerland

ABSTRACT In the kidney proximal tubule, acidification of the glomerular filtrate leads to an inhibition of inorganic phosphate (P_i) reabsorption by type II Na^+-coupled cotransporters (NaPi-II). As external pH also alters the divalent/monovalent P_i ratio, it has been difficult to separate putative proton interactions with the cotransporter from direct titration of divalent P_i, the preferred species transported. To distinguish between these possibilities and identify pH-sensitive transitions in the cotransport cycle, the pH-dependent kinetics of two NaPi-II isoforms, expressed in *Xenopus laevis* oocytes, were investigated electrophysiologically. At −50 mV, both isoforms showed >70% suppression of electrogenic response for an external pH change from 8.0 to 6.2, not attributable to titration of divalent P_i. This was accompanied by a progressive removal of steady-state voltage dependence. The NaPi-II-related uncoupled slippage current was unaffected by a pH change from 7.4 to 6.2, with no shift in the reversal potential, which suggested that protons do not function as substrate. The voltage-dependence of pre-steady-state relaxations was shifted to depolarizing potentials in 100 mM and 0 mM Na^+_{ext} and two kinetic components were resolved, the slower of which was pH-dependent. The changes in kinetics are predicted by a model in which protons interact with the empty carrier and final Na^+ binding step.

INTRODUCTION

The reabsorption of inorganic phosphate (P_i) from the glomerular filtrate occurs principally along the renal proximal tubule and is an essential means of controlling phosphate homeostasis. Up to 80% of P_i resorption is mediated by a secondary-active, electrogenic Na^+-coupled cotransport system located in the proximal tubule apical brush border membrane (for review see Murer et al., 1999). This system was identified through expression cloning (Magnanin et al., 1993) and comprises a unique family of proteins expressed in a number of mammalian and non-mammalian species.

Members of this family were originally classified as the type II Na^+/P_i cotransporters based on their molecular homology and similarity of functional properties (for review see Murer and Biber, 1996; Murer et al., 2000). More recently, this family has been subclassified into type IIa and type IIb (Hilfiker et al., 1998) based on the presence of unique structural motifs in the C-terminal of the protein. Type IIa are found exclusively in the mammalian renal cortex, whereas type IIb are ubiquitously distributed, but not expressed in the mammalian kidney. In non-mammalian species (e.g., flounder), type IIb is expressed in both kidney and small intestine (Werner et al., 1994; Kohl et al., 1996).

With respect to basic transport properties, the turnover rate of the type II system is a function of the concentration of the two substrates and membrane potential. Moreover, in the case of renal isoforms, P_i reabsorption rates are decreased by lowering the external (or luminal) pH. Because luminal pH can change by up to 1.0 pH units along the length of the proximal tubule according to the acid/base status of the organism (e.g., Gottschalk et al., 1960), this variable represents one means by which P_i reabsorption can be altered directly (for review see Knox and Haramati, 1985; Murer and Biber, 1992, 1996).

Under physiological conditions, P_i can exist in both monovalent and divalent forms in the physiological pH range (pK_a $[HPO_3^{2-}/HPO_4^-] \approx 6.8$). Therefore the observed pH-dependence of P_i reabsorption could be attributed to a P_i titration effect and/or an interaction of protons with the type II cotransporter. However, it has been experimentally difficult to identify which, if any, P_i species is preferentially transported and to unequivocally demonstrate interactions of protons with the cotransporter itself. Indirect evidence that protons can interact with the transporter protein has been obtained from studies involving the intact perfused proximal tubule and proximal tubule brush border membrane vesicle (BBMV) preparations. In the former case, Samarzija et al. (1982) reported a pH-dependence of the change in proximal tubular cell membrane potential in the presence of P_i (indicative of electrogenic transport), which could not be accounted for in terms of availability of one species of P_i alone. Quamme and Wong (1984) also concluded that elevated luminal H^+ ion concentration inhibits P_i influx by acting directly on the carrier. For the BBMV preparation, Burckhardt et al. (1981) concluded that the observed pH dependence arose from a direct action of protons on the cotransporter and that both monovalent and divalent P_i were transported depending on species availability. However, Cheng and Sacktor (1981) have presented evidence for preferential transport of divalent P_i using the renal BBMV preparation (see also Bindels et al. (1987)) and their findings also suggested a direct effect of H^+ ions on

Received for publication 13 October 1999 and in final form 22 March 2000.

Address reprint requests to Dr. Ian C. Forster, Physiologisches Institut, Universität Zürich, Winterthurerstrasse 190, CH-8057, Zürich, Switzerland. Tel.: 41-1-635-5059; Fax: 41-1-635-6814; E-mail: forster@physiol.unizh.ch.

© 2000 by the Biophysical Society

0006-3495/00/07/215/16 $2.00

the transport system. Finally, Amstutz et al. (1985) have proposed that the pH-dependence of P_i uptake in BBMVs most likely arises from protons competing for access to the Na^+ binding site(s).

One disadvantage of preparations of native renal membranes or renal cell lines is that contributions to the measured P_i transport by proteins other than NaPi-IIa/b cannot be excluded. For example, Bindels et al. (1987) reported two Na^+-dependent P_i transport systems having different pH sensitivities and affinities in the rat renal BBMV system. Furthermore, since type II Na^+/P_i cotransporters are electrogenic (Busch et al., 1994), membrane voltage necessarily plays a role in determining transport kinetics. The control of this parameter, which is not easily achieved with either the BBMV or intact proximal tubular preparation, is therefore essential to elucidate the mechanism underlying pH sensitivity. In this respect some aspects regarding pH dependence have already been addressed under more controlled experimental conditions. For example, from recent voltage clamp studies of renal type IIa Na^+/P_i cotransporters heterologously expressed in *Xenopus laevis* oocytes, Hartmann et al. (1995) found that lowering external pH shifted the apparent affinity for Na^+ (K_m^{Na}). Moreover, in the pH range 7.4–6.8, preferential transport of divalent P_i has been recently confirmed by simultaneous electrophysiological recording and tracer flux measurements on two type II Na^+/P_i cotransporter isoforms (Forster et al., 1999a). Finally, analyses of pre-steady-state charge movements, which reflect voltage-dependent transitions in the cotransport mechanism of the type II cotransporters (flounder NaPi-IIb, Forster et al. (1997a); rat NaPi-Iia, Forster et al. (1998)) have suggested that protons may also alter the voltage-dependence of the pre-steady-state relaxations. However, in both these studies the pH-sensitive transitions were not explicitly identified and their role in determining the overall pH dependency has remained uncertain.

The aim of this study was to characterize the pH dependency of two isoforms (rat, renal NaPi-Iia and flounder renal/intestinal NaPi-IIb) and thereby clarify the role of protons in modulating type II Na^+/P_i cotransporter kinetics. Both isoforms are known to exhibit a strong pH-dependence of the steady-state P_i transport (Magnanin et al., 1993; Werner et al., 1994). Cotransporters were expressed in *Xenopus* oocytes and transport kinetics assayed using the two-electrode voltage clamp technique. Interpretation of both steady-state and pre-steady-state behavior in terms of an ordered kinetic scheme for the type II Na^+/P_i cotransport system led to the identification of two partial reactions that are sensitive to external protons: the empty carrier, which determines the voltage-dependent kinetics, and the last Na^+ binding, which determines the apparent affinity for Na^+. Some of the material presented in this study has been reported in abstract form (Forster et al., 1997a).

MATERIALS AND METHODS

Oocytes

Stage V-VI oocytes from the clawed frog *Xenopus laevis* were prepared according to standard procedures and injected (50 nl injection volume) with ~10 ng/oocyte of cRNA encoding for either the rat renal cotransporter (*rat* NaPi-Iia, (Magnanin et al., 1993)) or the flounder renal cotransporter (*flr* NaPi-IIb (Werner et al., 1994)) 24–48 h after defolliculation, as previously described (Forster et al., 1997b, 1998). Cells were incubated at 16–18°C in modified Barth's solution (see below) and tested for expression 2–5 days after injection. Only cells having a resting membrane potential exceeding −20 mV and a leakage current not exceeding −50 nA at −50 mV were used for the subsequent experiments.

Electrophysiology and data acquisition

Oocytes were placed in a small recess in a Plexiglas superfusion chamber (volume 0.2 ml) and continuously superfused at 2–5 ml/min with the appropriate test solutions (see below). All superfusates were cooled to 18–20°C before entering the recording chamber.

Oocytes were voltage clamped using a custom-built two-electrode voltage clamp with active series resistance compensation to improve the clamping speed for pre-steady-state measurements. For assessing steady-state transport activity, currents were measured at a holding potential of −50 mV to reduce possible contamination from Ca^{2+}-activated Cl^- currents when the cells were subsequently depolarized. The exposure time to P_i was kept to a minimum (typically ≤ 20 s) to reduce possible intracellular accumulation of substrate. Current-voltage (*I-V*) curves were generated using a staircase protocol with 20-mV steps of 200-ms duration from −120 mV to +60 mV as previously described (Forster et al., 1998). All current recordings were filtered using an 8-pole Bessel filter (Frequency Devices, Model 902, Haverhill, MA) at a cutoff frequency less than twice the sampling frequency used. Data acquisition, voltage command generation, and solution valve control were performed using either a laboratory-built PC-compatible hardware and programmed as previously described (Forster et al., 1997b, 1998) or a Digidata 1200 system with pClamp v. 8.0 software (Axon Instruments, Foster City, CA) using the same experimental protocols.

Solutions and chemicals

All standard chemicals and reagents were obtained from Sigma or Fluka (Buchs, Switzerland).

The composition of the solutions used was as follows:

1. Oocyte incubation (modified Barth's solution) (mM): NaCl (88); KCl (1); $CaCl_2$ (0.41); $MgSO_4$ (0.82); $NaHCO_3$ (2.5); $Ca(NO_3)_2$ (2); TRIS (7.5); pH 7.6 and supplemented with antibiotics (10 mg/l penicillin, streptomycin);
2. Control superfusate, ND100, (mM): NaCl (100); KCl (2); $BaCl_2$ or $CaCl_2$ (1.8); $MgCl_2$ (1); Tris-HEPES (5-*N*-hydroxyethylpiperazine-*N*′-2,2-ethanesulfonic acid) (10) and adjusted to pH 7.4 with KOH. For other pH values, the following buffers were used: Tris (pH 8.0); PIPES (pH 6.8); and MES (pH ≤ 6.2). Pre-steady-state measurements were usually done with Ba^{2+} as the main divalent cation to reduce contamination from Ca^{2+}-activated Cl^- currents at depolarizing potentials and oscillatory Cl^- currents observed in some batches of oocytes at low pH (Woodward and Miledi, 1992). For solutions involving phosphonoformic acid (PFA), Ca^{2+} was used as the divalent cation because Ba^{2+} complexes with PFA;
3. Sodium substitution solutions: ND0 (0 mM Na^+) as for ND100, with equimolar substitution for NaCl by *N*-methyl-D-glucamine or choline chloride;
4. P_i test superfusate: control superfusate plus inorganic phosphate (P_i) as KH_2PO_4/K_2HPO_4, which was proportioned to give the required pH;

5. Butyrate solution: for acidifying oocytes, sodium butyrate (1 M stock) was added to the zero Na^+ superfusate (pH 6.2) to give concentrations in the range 10–30 mM sodium butyrate. pH was readjusted to ~6.2;
6. Phosphonoformic acid (PFA) was added to the superfusate from frozen stock aliquots (0.1 M) to give a final concentration of 3 mM; pH was readjusted to nominal value.

Intracellular pH measurements

Intracellular pH (pH_{int}) was monitored using a third micropipette inserted into the cell after stable voltage clamp recording conditions were established. To achieve voltage clamping of the cell at the same time as pH_{int} measurements, the voltage-sensing electrode of the voltage clamp was also used as the pH reference electrode. The pH electrode potential was measured using a laboratory-built unity gain electrometer amplifier incorporated in the electrode holder. The signals from the two electrodes were fed to a separate differential amplifier and the output continuously recorded on a chart recorder; pH-sensitive micropipettes were prepared as previously described (e.g., Choe et al., 1997). Briefly, borosilicate glass pipettes with an inner filament (GC150TF-10, Clark, Reading, UK) were pulled using a three-stage pulling process to give tips <0.2 μm in diameter. Electrodes were prepared by first silanizing for 10 min at 200°C using bis-di-(methylamino)-dimethylsilane (Fluka, Buchs, Switzerland) in a closed glass container and filled with the hydrogen ionophore I, cocktail B (Fluka) by capillary action and slight suction to a level of ~200 μm. Electrodes were then back-filled with a buffer solution containing (mM): KH_2PO4 (40), NaOH (23), and NaCl (15), pH 7.0. Before impaling the cell, the electrode was calibrated using ND100 test solutions of known pH at pH 7.4, 6.8, and 6.2, and a three-point calibration performed. At the end of an experiment, the reference and pH electrodes were withdrawn from the cell and the calibration procedure was repeated. The mean of the two measurements was used to estimate the pH. The deviation was typically <5% after up to 60 min recording.

Data analysis and curve-fitting

Nonlinear regression analysis was performed using Inplot v. 4.0 or Prism v. 2.0 software (Graphpad Inc., San Diego, CA). All data are shown as mean ± SEM (n), where n is the number of oocytes. Experimental protocols were repeated at least twice on different batches of oocytes from different frogs.

Steady-state inhibition

The pH-induced change in steady-state electrogenic response was quantified by fitting a form of the Hill equation to the data:

$$I_p/I_{pmax} = [H^+]^{n_h}/([H^+]^{n_h} + (K_i)^{n_h}) \quad (1)$$

where $[H^+]$ is the proton concentration; I_p is the steady-state P_i-induced current, I_{pmax} is the extrapolated maximum current, K_i is the proton concentration that gives a half-maximum response or apparent inhibition constant, and n_h is the Hill coefficient.

Pre-steady-state relaxations

Analysis was performed by fitting exponentials using a curve-fitting algorithm based on the Chebychev transformation (e.g., Axon Instruments, 1999) to estimate the relaxation time constant (τ). In cases where more than one component was clearly present, the main component was peeled off first with a single exponential fit. This method was found to be more reliable than multiple exponential fitting when the signal-to-noise ratio was poor or there was contamination from residual 50 Hz (see Forster and Greeff, 1992). First, a two-exponential fit was made to estimate the faster τ (τ_1). A single fit that commenced at $5 \times \tau_1$ after the step onset was then applied to the original record. The total charge (Q) was found by numerical integration of the NaPi-II associated relaxation.

To quantitate the voltage-dependence of Q and τ, we used nonlinear regression analysis to fit the following equations that are derived from a two-state Eyring-Boltzmann model for a charge of valency z that translocates between two states ($1 \Leftrightarrow 2$) over a symmetrical energy barrier (see Appendix). The time constant (τ) is given by:

$$\tau = 1/(k_{12}^o \exp(zeV/2kT) + k_{21}^o \exp(-zeV/2kT) \quad (2)$$

where V is the transmembrane voltage, e is the electronic charge, k is Boltzmann's constant, T is the absolute temperature, and k_{12}^o, k_{21}^o are the rate constants at $V = 0$ for the forward ($1 \Rightarrow 2$) and backward ($1 \Leftarrow 2$) transitions, respectively. For N cotransporters at any membrane voltage V, the charge (Q) is distributed according to the Boltzmann distribution: $Q = Q_{max}/(1 + \exp(-ze(V - V_{0.5})/kT))$, where Q_{max} ($= Nze$) is the maximum translocatable charge and $V_{0.5}$ is the voltage at which the apparent charge is distributed equally between states 1 and 2. Therefore, a voltage step from the holding potential (V_h) to any V moves an amount of charge:

$$Q(V - V_h) = Q_{max}/(1 + \exp(-ze(V - V_{0.5})/kT)) - Q(V_h) \quad (3)$$

and $Q(V_h)$ is the charge that has moved from the extreme hyperpolarizing potential to V_h.

External pH suppresses the type II Na^+/P_i cotransporter electrogenic response

Fig. 1 *A* illustrates the typical electrogenic response of oocytes expressing the type II Na^+/P_i cotransporter isoforms from rat (*rat* NaPi-IIa) and flounder (*flr* NaPi-IIb) when exposed to 1 mM total P_i at five external pH (pH_{ext}) values indicated and voltage clamped to −50 mV. The P_i-induced current (I_p) comprised an initial rapid inward phase, followed by a slower relaxation to the steady state. After removal of P_i, the current also showed a rapid decrease, followed by a slower return to the baseline. The slow phases of the electrogenic response have been previously reported (Forster et al., 1998) and are dependent on the superfusion conditions and accessibility of the oocyte membrane to the substrate in the recording chamber. For both isoforms there was a significant suppression of I_p at $pH_{ext} \leq 6.8$. The suppression of I_p was fully reversible (data not shown).

Fig. 1 *B* compares data pooled from a total of eight oocytes obtained from two donor frogs, which expressed the respective proteins and were measured under the above conditions. The peak I_p for each test $pH_{ext} < 7.4$ was normalized to I_p at $pH_{ext} = 7.4$. Although both isoforms showed similar pH-dependent suppression of I_p, *rat* NaPi-IIa gave a consistently larger suppression at all $pH_{ext} < 7.4$. The inhibitory effects of pH_{ext} were quantitated by fitting Eq. 1 to the pooled data. For both isoforms, a Hill coefficient $n_h < -1$ was obtained (n_h (*rat* NaPi-IIa) $= -1.5 \pm 0.2$; n_h (*flr* NaPi-IIb) $= -2.1 \pm 0.1$), which suggested that the inhibition was the result of the interaction of > 1 proton with the protein. The corresponding apparent inhibition constants (K_i) were similar for each isoform (K_i (*rat* NaPi-IIa) $= 0.42 \pm 0.01$ μM; K_i (*flr* NaPi-IIb) $= 0.31 \pm 0.02$ μM).

Under these test conditions, total P_i was constant (1 mM) for all pH_{ext} values. However, if we assume $pK_a = 6.8$ for P_i to take account of the ionic strength of the superfusate, the divalent/monovalent P_i ratio would therefore change from ~16:1 at $pH_{ext} = 8.0$ to 0.25:1 at $pH_{ext} = 6.2$, as given by the Henderson-Hasselbach equation. Indeed, divalent P_i has been shown to be the preferred species transported (Forster et al., 1999a) for both these isoforms for pH_{ext} in the range 6.8–7.4. Therefore, the dependence on pH_{ext} might be attributed to the titration of divalent versus monovalent P_i in the superfusion medium. For this to be the case, we would predict that the pH-dependent inhibition would simply reflect the availability of diva-

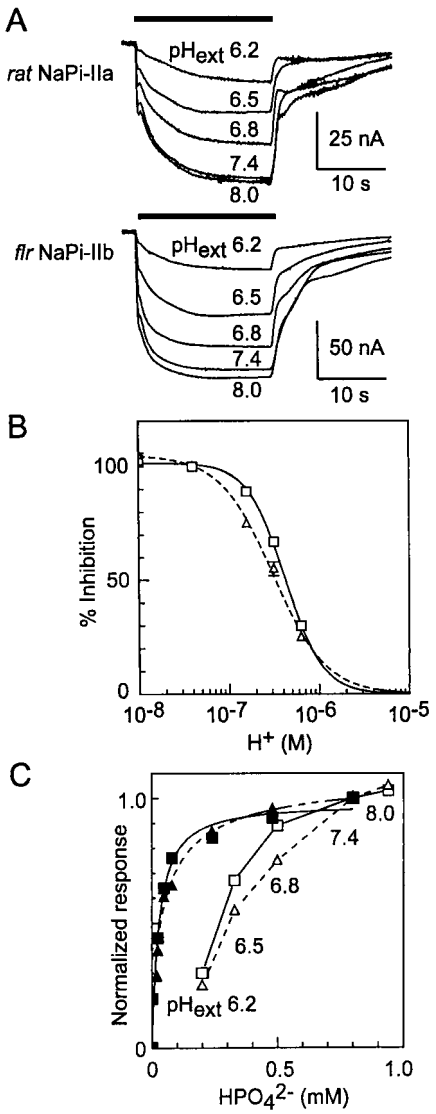

FIGURE 1 pH-dependence of P_i-activated currents in the steady state. (*A*) Typical recordings from oocytes expressing the rat renal isoform (*rat* NaPi-IIa) (*top*) and flounder renal/intestinal isoform (*flr* NaPi-IIb) (*bottom*). In each case, the respective oocyte was voltage clamped to −50 mV, and first superfused with a control solution that was adjusted to the respective test pH before a 20-s application of a P_i-containing solution (1 mM), indicated by the bar, at the same pH. Baseline shifts have been adjusted to indicate only the P_i-induced current (I_p). The slower relaxation to the steady-state level is a function of the superfusion conditions and oocyte unstirred layer effects. Note the different current scales for the two isoforms. (*B*) Percent inhibition of I_p as a function of H^+ (M) for each isoform, normalized to the respective response at pH 7.4 under the same recording conditions as in (*A*): *rat* NaPi-IIa (△; *dashed line*) and *flr* NaPi-IIb (□, *solid line*). Each point is the mean of eight oocytes. SEM values smaller than symbol size are not shown. (*C*) Normalized P_i dose-response data and corresponding fit to Hill equation for a typical oocyte expressing *rat* NaPi-IIa (▲, *dashed line*) and *flr* NaPi-IIb (■, *solid line*) at −50 mV and pH 7.4 obtained from previous studies (Forster et al., 1997b, 1998). The abscissa position of each data point has been readjusted to correspond to the amount of divalent P_i present at pH_{ext} = 7.4. Both the curves and data for each isoform have been normalized to the response at 1 mM total P_i (equivalent to 0.8 mM HPO_4^{2-} at pH 7.4). Superimposed on these data are the normalized, mean values from (*B*) plotted according to the titration of divalent P_i with pH_{ext}: *rat* NaPi-IIa (△, *dashed line*) and *flr* NaPi-IIb (□, *solid line*).

lent P_i as pH_{ext} changed, and should therefore superimpose on the P_i activation curve for type II Na^+/P_i cotransport.

To test this hypothesis, we compared the P_i activation curves for each isoform with the pH-inhibition data, as shown in Fig. 1 *C*. Each data set was normalized to the response at pH_{ext} = 7.4 and 1 mM total P_i (equivalent to 0.8 mM HPO_4^{2-}). The P_i activation data (*filled symbols*) are shown for one representative cell expressing each isoform, obtained from previously published data (Forster et al., 1997, 1998), at −50 mV and plotted against the equivalent divalent P_i concentration. The pH-inhibition data of Fig. 1 *B* (*open symbols*) were replotted against the divalent P_i concentration determined from the Henderson-Hasselbach equation. The two data sets deviated significantly as divalent P_i concentration decreased. For example, with 1 mM total P_i, a decrease in pH_{ext} from 7.4 to 6.2 corresponds to a decrease in HPO_4^{2-} from 0.8 mM to 0.2 mM. According to the P_i activation data for each isoform, this gave <20% suppression of the P_i-induced response, whereas the pH inhibition data showed 70% suppression. This result supported the notion that protons per se interact with the cotransporter and established that titration of P_i could not alone account for the suppression of the steady-state response.

The above measurements were performed at a holding potential, V_h = −50 mV. Because type II Na^+/P_i cotransporters display voltage-dependent behavior in the steady state, we investigated the effect of pH_{ext} changes on the steady-state current-voltage (*I-V*) curves (see Materials and Methods) under the same conditions. Fig. 2 *A* shows the original response of an oocyte expressing *flr* NaPi-IIb to a voltage staircase from −120 mV to +60 mV in the presence and absence of 1 mM total P_i at pH_{ext} = 7.4 and 6.2. Whereas at pH_{ext} = 7.4 there was an obvious deviation in two current records induced by P_i at more hyperpolarizing potentials, for pH_{ext} = 6.2, the current records were approximately parallel over the voltage range $-120 \le V \le +40$ mV. P_i-dependent current-voltage (*I-V*) relations were obtained by subtracting the two staircase responses. Representative *I-V* data, obtained from oocytes expressing *rat* NaPi-IIa and *flr* NaPi-IIb, are shown in Fig. 2 *B* for four pH_{ext} values. As pH_{ext} decreased, I_p also decreased for all $V < 0$ mV. Moreover, a voltage-independent rate-limiting behavior was observed, which was reflected in the flattening of the *I-V* curves at hyperpolarizing potentials, i.e., a maximum transport rate at 100 mM Na^+ was approached that depended on pH_{ext}. As pH_{ext} decreased, this voltage-independent behavior extended over a wider potential range, so that at pH_{ext} = 6.2, I_p was essentially voltage-independent for $-100 \text{ mV} < V < 0$ mV, as indicated from the original staircase induced currents. The small upward deflection at more hyperpolarizing potentials was also a reproducible feature of the *I-V* curves for both isoforms. The progressive flattening of the *I-V* curves as pH_{ext} decreased suggested that protons are also able to alter the voltage-dependent kinetics of both cotransporter isoforms in a dose-dependent manner.

Using the BBMV preparation, it has been reported that an outwardly directed pH gradient can stimulate P_i transport (Sacktor and Cheng, 1981; Strévey et al., 1990). To investigate whether this could also occur for heterologously expressed type II Na^+/P_i cotransporters, we acidified the oocyte interior using sodium butyrate. Internal pH (pH_{int}) was continuously monitored using a third micropipette containing a pH-sensitive cocktail. The pH electrode was first calibrated in test solutions before insertion in the cell (see Materials and Methods). After membrane penetration, for both noninjected and injected cells, the potential of the pH electrode was insensitive to changes in the pH_{ext}. Fig. 3 *A* shows the typical time course for acidification of an oocyte expressing *rat* NaPi-IIa. The corresponding P_i-activated steady-state current responses at the time points indicated (1–4) on the pH record are shown in Fig. 3 *B*. In each case the P_i response was measured with the standard external conditions (ND100, pH_{ext} 7.4). These data indicated that for an internal acidification of ~0.6 pH units, the

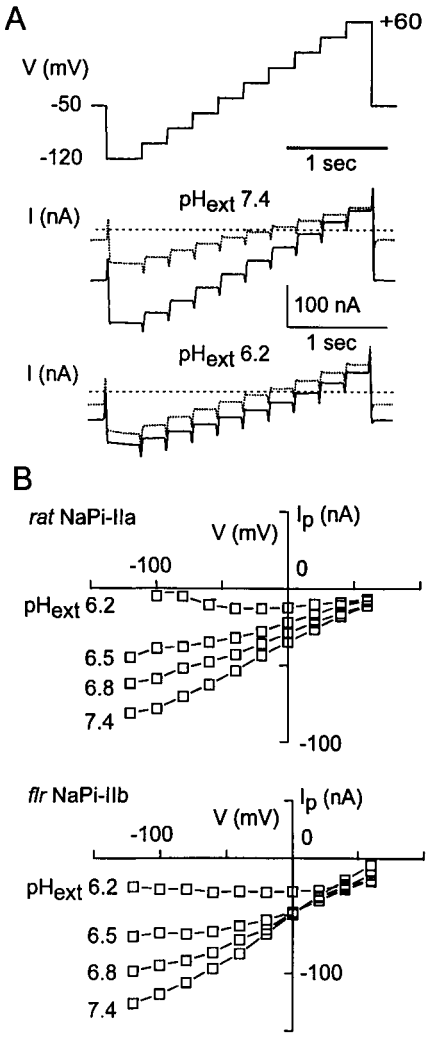

FIGURE 2 Dependence of steady-state current-voltage (*I-V)* relation on pH_{ext}. (*A*) Original current records obtained from an oocyte expressing *flr* NaPi-IIb in response to the voltage staircase (*upper trace*). The corresponding current under control conditions (ND100, pH_{ext} = 7.4 or 6.2) (*dotted traces*) and the current when the holding current had reached a steady state with P_i (1 mM, total) superfusion (*solid traces*) are shown for pH_{ext} = 7.4 and 6.2, as indicated. Dotted lines indicate zero current level at each pH_{ext}. The current spikes at the beginning of each step result from pre-steady-state charge movements in the absence of P_i that are revealed by the subtraction procedure. (*B*) Current-voltage (*I-V*) curves for representative oocytes expressing *rat* NaPi-IIa (*top*) and *flr* NaPi-IIb (*bottom*) at different pH_{ext} values indicated. Each point represents the P_i-induced steady-state current (I_p) found by subtracting control and P_i records such as shown in (*A*) and then determining the steady-state current at during each potential interval.

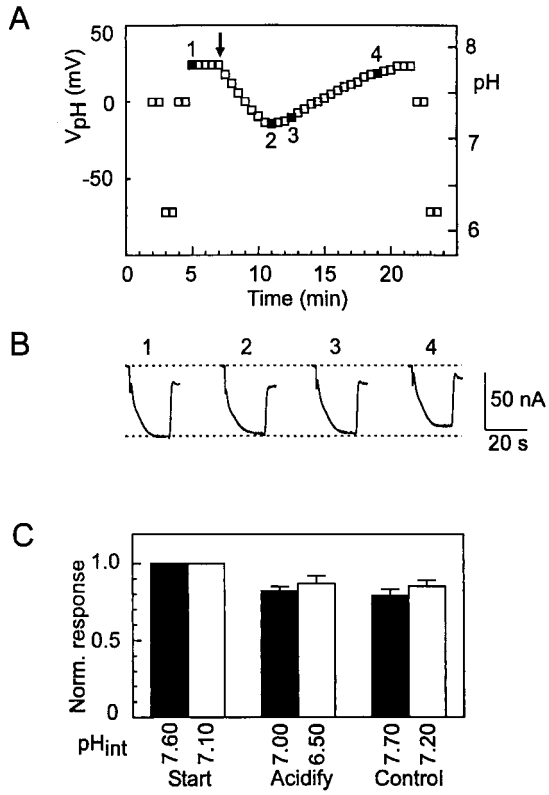

FIGURE 3 The effect of intracellular acidification on steady-state response. (*A*) Time course of acidification of a typical oocyte expressing *rat* NaPi-IIa. Each point is a measurement of potential at the pH electrode (*left ordinate*) and equivalent pH (*right ordinate*) based on calibration in test solutions at pH_{ext} = 7.4 and 6.2 before and after the experiment, indicated by separate points. At the times indicated by the filled points, the P_i-activated electrogenic response was measured as shown by the original records in (*B*). There was no significant change in the response over the course of the experiment. (*C*) Pooled data from two separate experiments showing the variation in P_i-induced response (pH_{ext} = 7.4) for four oocytes expressing the *rat* NaPi-IIa (*filled bars*) and *flr* NaPi-IIb (*open bars*) isoforms measured at the start, during acidification, and after recovery to normal pH_{int}. The pH_{int} values at each measurement are indicated on the abscissa.

P_i-activated response remained essentially constant. This experiment was also performed with oocytes expressing *flr* NaPi-IIb and, like *rat* NaPi-IIa, no stimulation of the P_i-activated current was observed (data not shown). Pooled results for oocytes expressing each isoform are shown in Fig. 3 *C*. A consistent feature of these experiments was the small (≈20%) decrease in the response after initial acidification, which remained after restoration of the initial conditions. Moreover, we observed no alteration in the ratio of the P_i-induced response at pH_{ext} = 7.4 to that at pH_{ext} = 6.2 after internal acidification (*rat* NaPi-IIa, n = 2). Apart from the response "rundown," which was within the limits normally experienced with long-term superfusion of type II Na^+/P_i cotransporters (e.g., Forster et al., 1999b), these results indicated that under our experimental conditions, only changes in pH_{ext} altered the P_i-induced electrogenic response.

Interaction of protons with uncoupled Na^+ slippage

In general, cotransport mode kinetics are a function of all the rate constants of transitions that lead to the fully loaded carrier state (see kinetic scheme, Fig. 9). To identify the transition or transitions involved in proton-NaP_i-II interactions, we next investigated whether pH_{ext} affected the uncoupled Na^+ slippage current in the steady-state (transition 2 ⇔ 7, Fig. 9). For *rat* NaPi-IIa it has been shown that in the absence of P_i, the Na^+/P_i cotransport inhibitor phosphonoformic acid (PFA) suppresses a Na^+-dependent "leak"

or slippage current, the magnitude of which correlates with I_p (Forster et al., 1998). We therefore used PFA as an inhibitor to characterize the slippage behavior.

Fig. 4 *A* shows the electrogenic response induced by 1 mM (total) P_i and 3 mM PFA at pH_{ext} = 7.4 and 6.2 for a representative oocyte that expressed *rat* NaPi-IIa. At pH_{ext} = 7.4, $I_p \approx -100$ nA and the change in holding current induced by PFA (I_{PFA}) = +7 nA. When the control solution was changed to pH_{ext} = 6.2, the baseline holding current decreased by 8 nA. Relative to the new baseline at pH_{ext} = 6.2, $I_p = -27$ nA and $I_{PFA} = +10$ nA. As the continuous recording shows, the changes in holding current effected by pH_{ext} and PFA were repeatable. For a noninjected oocyte from the same batch, P_i and PFA induced small (<4 nA) changes in holding current, and there was a consistent endogenous response to changes in the pH of the control solution. We obtained qualitatively similar results for the *flr* NaPi-IIb isoform; however, the PFA-sensitive currents were >2-fold smaller despite up to 5-fold larger P_i-induced currents under the same conditions. Fig. 4 *B* summarizes pH_{ext} and PFA-induced changes in holding current (ΔI_h) after the solution changes indicated on Fig. 4 *A*, for noninjected and *rat* NaPi-IIa expressing oocytes from the same donor frog (n = 6). Although I_{PFA} was significantly larger than the endogenous response for the NaPi-IIa expressing oocytes at each pH_{ext}, the endogenous response to the pH change was not significantly different from that of *rat* NaPi-IIa (Student's *t*-test, $p < 0.05$). Moreover, the small increase in the mean I_{PFA} at pH_{ext} = 6.2 was also insignificant ($p < 0.05$). The larger SEM for the *rat* NaPi-IIa pool could be accounted for by the variation in expression levels, which was reflected in I_p (−110 ± 8 nA).

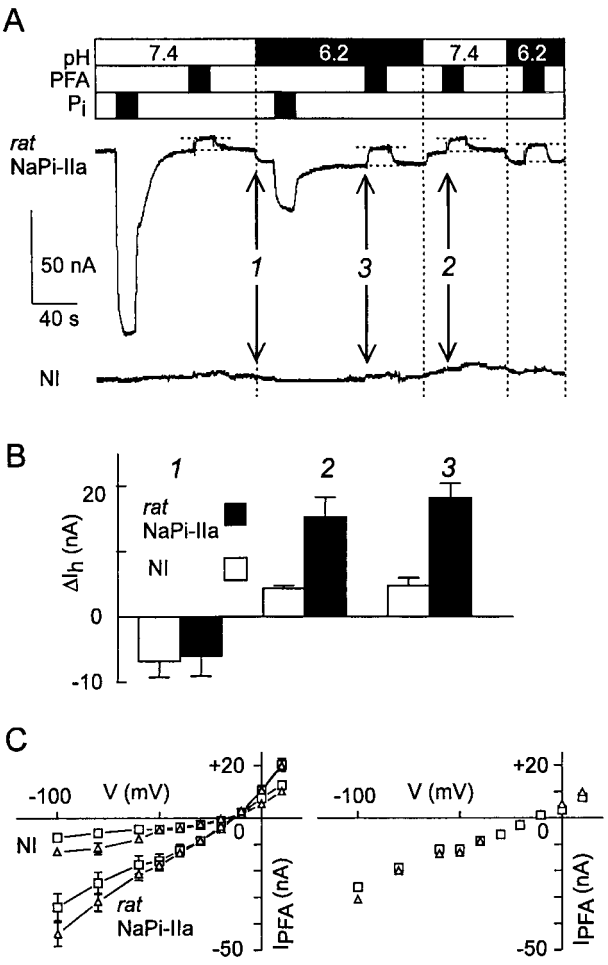

FIGURE 4 The effect of pH_{ext} on Na^+-dependent slippage for oocytes expressing rat NaPi-Iia. (*A*) Continuous recording of an oocyte that expressed *rat* NaPi-IIa (*top trace*) and a noninjected (NI) oocyte from the same donor frog (*bottom trace*) with substrate and pH_{ext} indicated by bars. Changes in holding current induced by PFA are indicated by horizontal dashed lines. Vertical dotted lines indicate when the superfusate pH changed. The Na^+ concentration under control conditions and with P_i was increased by 9 mM to compensate for the PFA (see Materials and Methods). Arrows indicate changes in holding current shown as pooled data in (*B*). (*B*) Pooled data that summarize the changes in holding current (ΔI_h) at points shown in (*A*) induced by pH_{ext} (1), PFA at pH_{ext} = 7.4 (2), and PFA at pH_{ext} = 6.2 (3), for noninjected oocytes (NI) and oocytes expressing *rat* NaPi-IIa from the same donor frog (n = 6) at V_h = −50 mV. (*C*) *Left*: current-voltage (*I-V*) curves that show the steady-state voltage-dependence of the PFA-sensitive current (I_{PFA}) recorded from the same oocytes as in (*B*): pH_{ext} = 7.4 (□); pH_{ext} = 6.2 (△). Each data point represents the steady-state current at the particular voltage determined by subtracting the current with PFA (3 mM) from the current without PFA at the respective pH_{ext}. *Right*: *I-V* curves for pH_{ext} = 7.4 (□) and pH_{ext} = 6.2 (△) showing mean I_{PFA} after subtraction of the mean I_{PFA} from noninjected oocytes.

To further characterize the slippage behavior, we generated *I-V* curves from the same pools of oocytes (Fig. 4 *C*, *left*). Under the assumption that the endogenous response to PFA remained the same when oocytes expressed *rat* NaPi-IIa, we subtracted these data from the mean *rat* NaPi-IIa response at each test potential to estimate the uncontaminated slippage current (Fig. 4 *C*, *right*). There was no significant difference in I_{PFA} at the two pH values and, moreover, the reversal potential (E_r) of I_{PFA} was not significantly altered by pH_{ext} (E_r = −12 mV (pH_{ext} = 7.4); (−10 mV) pH_{ext} = 6.2). Finally, for oocytes that expressed *rat* NaPi-IIa and superfused in nominal 0 mM Na^+_{ext} (ND0), application of P_i (1 mM, total) at either pH_{ext} = 7.4 or 6.2 did not induce a significant (<2 nA) change in holding current at −50 mV at the respective pH_{ext} (data not shown). This result suggested that protons do not substitute for Na^+ as the co-substrate.

External pH modulates pre-steady-state relaxations in the presence and absence of external Na^+

Further insight into the interaction of protons with the voltage-dependent kinetics of type II Na^+/P_i cotransporters is reflected in the time course and magnitude of pre-steady-state relaxations induced by voltage steps (Forster et al., 1997b, 1998). Voltage-dependent transitions, which have been attributed to the empty carrier and Na^+ binding, respectively, contribute to these charge movements. To identify which, if any, of the partial reactions in the transport cycle was pH-sensitive, we recorded pre-steady-state relaxations with different pH_{ext} and superfusion solutions.

Fig. 5 *A* shows a representative family of pre-steady-state relaxations recorded from an oocyte expressing *flr* NaPi-IIb, recorded first at pH_{ext} = 7.4 and then repeated at pH_{ext} = 6.2 in the presence of 100 mM Na^+_{ext} (ND100 solution). In each case, the membrane voltage was stepped from a holding potential V_h = −100 mV to test potentials in the range −180 to +60 mV. The time course of these records suggested that the reduction in pH_{ext} slowed the relaxations for steps to depolarized potentials. Moreover, less charge was evoked for steps in the hyperpolarizing direction ($V < V_h$). The effect of pH_{ext} on the pre-steady-state charge movements was reversible, which indicated that exposure to low pH_{ext} superfusates did not result in permanent modification of the *flr* NaPi-IIb protein (data not shown). The relaxations were completely suppressed when the same oocyte was superfused with 3 mM PFA (100 mM Na^+, pH_{ext} = 7.4 and 6.2), as shown in this case for pH_{ext} = 7.4. For these superfusion conditions, the remaining current transients were indistinguishable from those obtained from a noninjected oocyte in the absence of PFA (data not shown). We assumed that

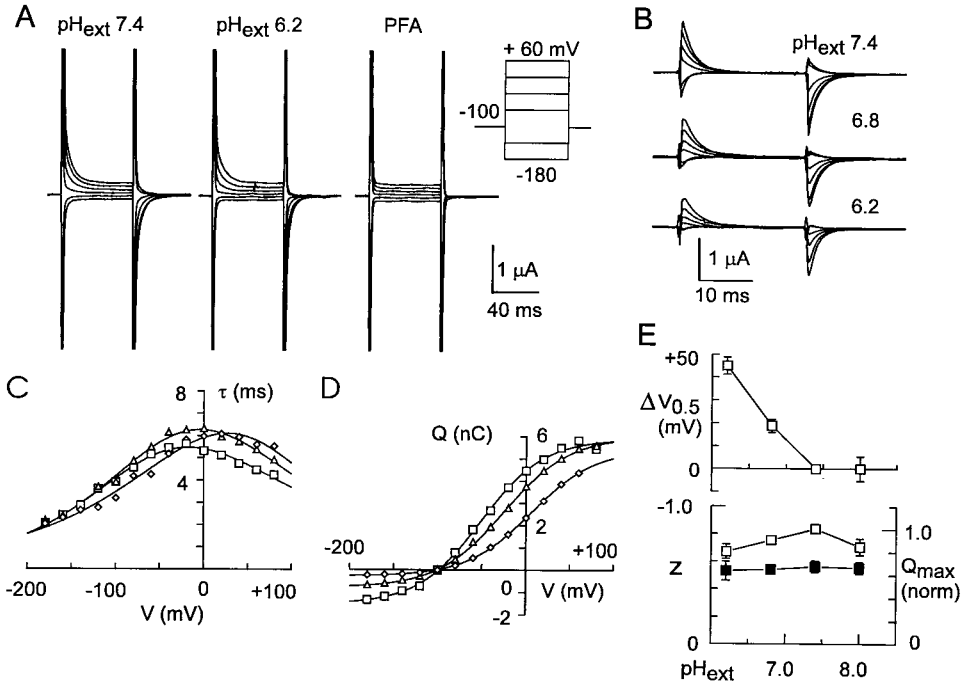

FIGURE 5 Pre-steady-state relaxations with 100 mM external Na^+ are sensitive to pH_{ext}. (*A*) Family of representative pre-steady-state relaxations induced by voltage steps in the range −180 mV to +60 mV from a holding potential of −100 mV, recorded from an oocyte expressing the *flr* NaPi-IIb isoform. Oocyte was superfused with 100 mM Na^+ (ND100) adjusted to pH 7. 4 (*left*) or pH 6.2 (*center*). In the presence of 3 mM phosphonoformic acid (PFA) (pH 7.4) (*right*), the relaxations are fully suppressed. Each record is the average of four sweeps, low-pass filtering at 500 Hz, sampling 50 μs/point. (*B*) Difference records from the same cell as in (*A*), obtained by subtracting the PFA record from the respective record at the indicated test pH. Records are shown for steps to −180, −140, −60, −20, +20, +60 mV from a holding potential of −100 mV. (*C*) Voltage-dependence of the time constant (τ) associated with the relaxations in (*B*) for pH_{ext} = 7.4 (□), 6.8 (△), and 6.2 (◇). The solid lines are fits to the data using Eq. 2 (see Materials and Methods). The fit parameters for this cell (pH_{ext} in parentheses) were k^o_{12} (s^{-1}): 82 (7.4), 68 (6.8), 57 (6.2); k^o_{21} (s^{-1}): 69 (7.4), 79 (6.8), 97(6.2); *z*: −0.50 (7.4), −0.48 (6.8), −0.42 (6.2). (*D*) Voltage-dependence of the corresponding charge movement for the same cell as in (*A*) for pH_{ext} = 7.4 (□), 6.8 (△), and 6.2 (◇). The solid lines are fits to Eq. 3 (see Materials and Methods). The fit parameters at the respective pH_{ext} (in parentheses) were $V_{0.5}$: −15 mV (7.4), +1.5 mV (6.8), +31 mV (6.2); *z*: −0.59 (7.4), −0.60 (6.8), −0.55 (6.2); Q_{max}: 7.4 nC (7.4), 6.7 nC (6.8), 5.7 nC (6.2). (*E*) Pooled results showing dependence of fit parameters on pH_{ext} for fits to the *Q-V* curves (Eq. 3) for oocytes expressing the *flr* NaPi-IIb isoform (n = 8). *Top*: change in $V_{0.5}$ vs. pH_{ext} relative to $V_{0.5}$ at pH_{ext} = 7.4; *bottom*: *z* (■) (*left ordinate*) and Q_{max} (□) (*right ordinate*), normalized to estimated Q_{max} at pH_{ext} = 7.4. Data points joined by straight lines for visualization.

these transients represented the nonspecific charging of the oocyte membrane and we subtracted the PFA records from the respective test records as shown in Fig. 5 *B*. This procedure eliminated the contamination of the endogenous capacitive component and thereby allowed us to observe more clearly the pH-dependence suggested from the original records. We also confirmed that noninjected oocytes from the same batch of cells did not show any detectable change in the endogenous charging transient under the same superfusion conditions. This was a further indication that the subtracted traces represented only charge movements resulting from the expression of NaPi-II protein. The subtracted records confirmed that as pH_{ext} decreased, the kinetics of the relaxations changed, as observed in the raw data. Under the same recording and superfusion conditions, the *rat* NaPi-IIa isoform gave qualitatively similar results (data not shown).

To quantify these changes, a single exponential was fit to each subtracted relaxation to give the relaxation time constant (τ) as a function of membrane potential as shown in Fig. 5 *C*. There was a progressive shift in the maximum of the τ-*V* curves toward depolarizing potentials as pH_{ext} decreased and a significant increase in τ for $V > 0$. The apparent charge movement (*Q*) was obtained by quantitating the area under each relaxation (average of ON and OFF charges) (Fig. 5 *D*). These data showed a concomitant shift toward depolarizing potentials and more saturation in the hyperpolarizing region as pH_{ext} decreased.

The effects of pH_{ext} on the pre-steady-state relaxations were further quantitated by fitting a Boltzmann function (Eq. 3) to the *Q-V* data obtained from two batches of oocytes expressing *flr* NaPi-IIb and the fit parameters were pooled, as summarized in Fig. 5 *E*. To account for variations in functional expression levels between oocytes we normalized Q_{max} to the value at pH_{ext} = 7.4 for each oocyte. We also found that the estimates for $V_{0.5}$ varied between oocytes, particularly for oocytes from different batches. For example, for five cells at pH_{ext} = 7.4, $V_{0.5}$ ranged from −3 mV to −25 mV. However, as pH_{ext} decreased, the shift in $V_{0.5}$ relative to the value at pH_{ext} = 7.4 was a consistent trend for all oocytes examined, and therefore the pooled data for $V_{0.5}$ were expressed relative to the individual value at pH_{ext} = 7.4. We observed little change in the fit parameters for pH_{ext} = 8.0 and pH_{ext} = 7.4, and the apparent valency (*z*) and the total charge movement (Q_{max}) remained essentially constant over the whole pH range tested. These data suggested the existence of a proton-dependent modulatory mechanism, whereby the voltage-dependence of the charge movement was altered without changing its valency.

Pre-steady-state relaxations result from charge movements attributable to the binding/unbinding of Na^+ and the translocation of charges associated with the empty carrier. Consequently, from the above data it was difficult to distinguish between proton interactions with either or both transitions. Therefore, we repeated the above protocol in the nominal

absence of external Na^+ (ND0 superfusate). As shown in Fig. 6 *A*, for representative oocytes expressing each isoform, voltage steps induced pre-steady-state relaxations when superfused in ND0 at $pH_{ext} = 7.4$. When pH_{ext} was decreased to 6.2, the relaxations became noticeably slower at depolarizing potentials. At $pH_{ext} = 5.0$ the transient currents were indistinguishable from those obtained when superfusing with ND100 + 3 mM PFA (compare with Fig. 5 *A*). To better visualize the effect of changing pH_{ext} in ND0 solution, we subtracted the response at $pH_{ext} = 5.0$ from the responses for $pH_{ext} = 7.4$, 6.8, 6.2, and 5.6, respectively, at each test potential. Typical difference records for the two isoforms are shown in Fig. 6 *B*, together with records from a noninjected oocyte from the same batch, which showed no significant charge movement over the same time interval. The PFA-sensitive relaxations for superfusion in ND100, from the same cells, are superimposed on the subtracted record for ND0 ($pH_{ext} = 7.4$). These data indicated that superfusion in ND0 at $pH_{ext} = 7.4$ led to a detectable suppression of the main relaxation. The initial amplitude of the remaining charge movement was further suppressed as pH_{ext} was decreased from 7.4 to 5.6. Moreover, for both isoforms, the time course of the relaxations suggested that at least two relaxations were present, the slower of which became more prominent as pH_{ext} decreased.

Because charge movements associated with other membrane proteins might also contribute to, or even account for, these transient currents, we also confirmed that these charge movements recorded in ND0 were associated with functional NaPi-II protein. As shown in Fig. 7 *A* for 13 oocytes expressing *flr* NaPi-IIb, there was a clear correlation between the charge movement in the presence (Q^{100}) and absence (Q^0) of Na^+_{ext} for the same cell. For each oocyte tested, these charge movements were quantitated for voltage steps from $V_h = -100$ mV to 0 mV and +60 mV. We have previously reported that in 100 mM Na^+_{ext}, the magnitude of the charge movements correlates with the magnitude of the steady-state current (Forster et al., 1997b, 1998). Therefore the correlation between Q^{100} and Q^0 shown in Fig. 7 *A* strongly suggested that we had detected a charge movement associated with functional *flr* NaPi-IIb in the nominal absence of external substrates.

For both isoforms at $pH_{ext} = 7.4$, the *Q-V* data (*boxed insets*, Fig. 7 *B*) for the subtracted charge also showed a voltage-dependence that was qualitatively similar to that for 100 mM Na^+_{ext} with saturation at the potential extremes. Moreover, as pH_{ext} decreased, there appeared to be more saturation at hyperpolarizing potentials and less saturation at depolarizing potentials. This behavior suggested that pH_{ext} induced a shift of the charge distribution. We were unable to confirm whether saturation also occurred at $pH_{ext} = 5.6$, because of contamination from endogenous Cl^- currents for test potentials exceeding +100 mV.

To visualize this effect better, we fit Eq. 3 to these data and translated the fitted curves by the predicted $Q(V_h)$ (see Eq. 3) together with the data points so that the curves superimposed at extreme hyperpolarizing potentials. At $pH_{ext} = 5.6$ the lack of saturation at positive potentials prevented a free fit of Eq. 3 to be made, and *z* was constrained to the value predicted from the fit at $pH_{ext} = 7.4$. Table 1 summarizes the fitting results pooled from oocytes that expressed each isoform (*rat* NaPi-IIa ($n = 3$); *flr* NaPi-IIb ($n = 6$). As for the case with ND100 superfusion, to account for variations in functional expression levels we normalized the Q_{max} estimates for each cell to the value at $pH_{ext} = 7.4$. Similarly, we observed that the absolute $V_{0.5}$ obtained from the fit varied, particularly between batches of

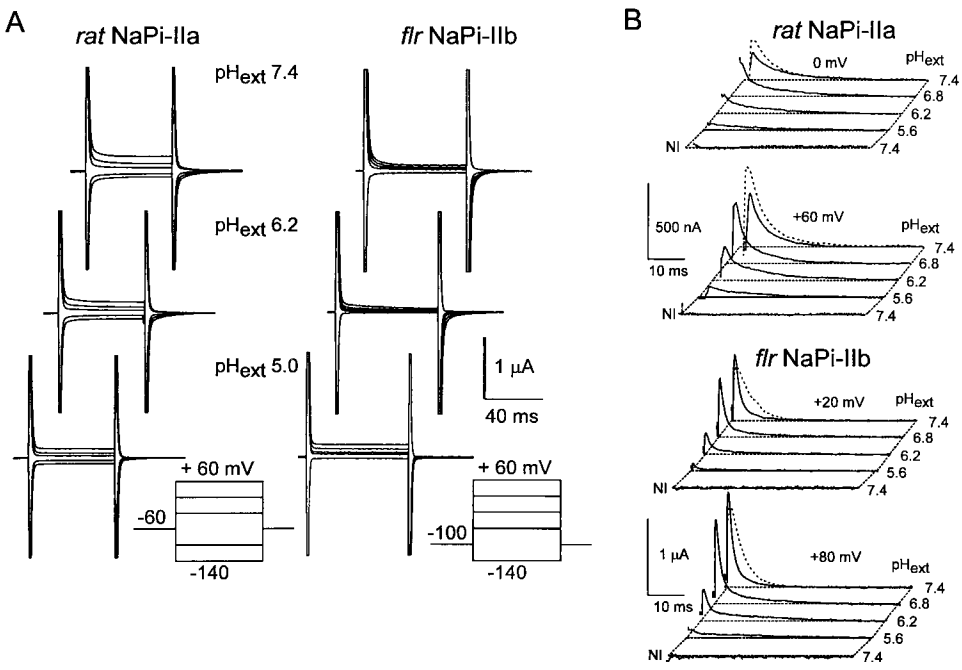

FIGURE 6 External pH modulates the voltage-dependence of pre-steady-state relaxations in 0 mM external Na^+. (*A*) Representative pre-steady-state relaxations recorded from oocytes expressing *rat* NaPi-IIa and *flr* NaPi-IIb superfused in ND0 at $pH_{ext} = 7.4$ (*top*), 6.2 (*middle*), and 5.0 (*bottom*). For *rat* NaPi-IIa, $V_h = -60$ mV and traces are shown for steps to −140, −100, −20, +20, and +60 mV. For *flr* NaPi-IIb, $V_h = -100$ mV and traces are shown for steps to −140, −60, −20, +20, and +60 mV. Each trace is the result of fourfold averaging and filtering at 500 Hz. (*B*) pH-dependent charge movements evoked by steps to the indicated test potentials for the same oocytes as in (*A*), after subtracting the corresponding responses at $pH_{ext} = 5.0$ from the records at $pH_{ext} = 7.4$, 6.8, 6.2, and 5.6, respectively. For comparison purposes, the response in ND100, pH_{ext} 7.4, with the PFA response subtracted (*dotted lines*) is superimposed on the response in ND0, $pH_{ext} = 7.4$. NI indicates the response for a noninjected oocyte from the same donor frog at $pH_{ext} = 7.4$, with the response at $pH_{ext} = 5.0$ subtracted. The difference records have been partially blanked for the first 1–1.5 ms during the charging period of the oocyte membrane capacitance.

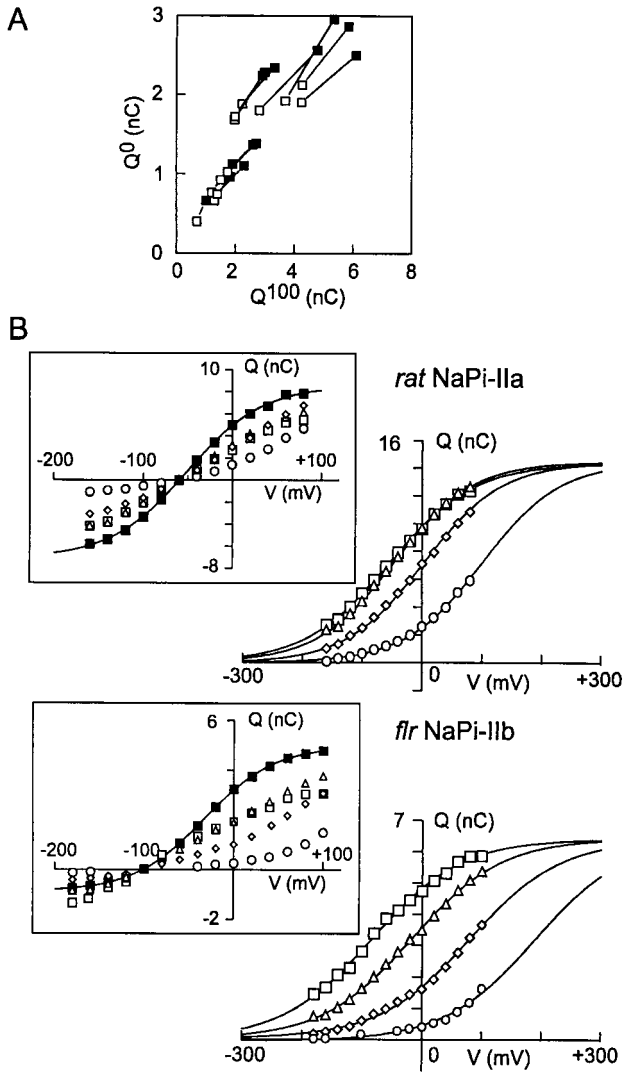

FIGURE 7 Kinetic properties of pH-dependent charge movements in 0 mM Na_{ext}. (*A*) Correlation between the charge induced by voltage steps to 0 mV (□) and +60 mV (■) from $V_h = -100$ mV for 13 representative oocytes expressing *flr* NaPi-IIb from 3 donor frogs in 100 mM Na^+_{ext} (Q^{100}) and 0 mM Na^+_{ext} (Q^0) ($pH_{ext} = 7.4$). Each pair of symbols joined by a line represents charge movements from the same oocyte. (*B*) Steady-state charge distribution (*Q-V*) for the two representative oocytes expressing *rat* NaPi-IIa (*top*) and *flr* NaPi-IIb (*bottom*) for the following superfusion conditions: ND100, $pH_{ext} = 7.4$ (■); ND0, $pH_{ext} = 7.4$ (□); 6.8 (△); 6.2 (◇); and 5.6 (○). Note that the holding potential (V_h) for *rat* NaPi-IIa = −60 mV and for *flr* NaPi-IIb, $V_h = -100$ mV. Equation 3 was fit to the data for ND0 superfusion shown in the insets and the data and fitted curves were translated vertically by $Q(V_h)$ so that the curves superimposed at the hyperpolarizing limit. The fit parameters at the respective pH_{ext} (in parentheses) were for *rat* NaPi-IIa: $V_{0.5}$: −54 mV (7.4), −46 mV (6.8), +0.5 mV (6.2), +101 (5.6); *z*: −0.35 (7.4), −0.38 (6.8), −0.35 (6.2), −0.35* (5.6); Q_{max}: 14.4 nC (7.4), 14.7 nC (6.8), 15.1 nC (6.2), 14.3 (5.6), and for *flr* NaPi-IIb: $V_{0.5}$: −84 mV (7.4), +7.1 mV (6.8), +80 mV (6.2), +188 (5.6); *z*: −0.33 (7.4), −0.29 (6.8), −0.33* (6.2), −0.33* (5.6); Q_{max}: 6.4 nC (7.4), 6.5 nC (6.8), 6.4 nC (6.2), 6.4* (5.6). Parameters marked * were constrained for the fit.

oocytes. However, the change in $V_{0.5}$ relative to the value at $pH_{ext} = 7.4$ was consistent among oocytes. Moreover, both normalized Q_{max} and the apparent valency (*z*) showed little dependence on pH_{ext}.

Further characterization of the charge movements was done by fitting exponential functions to the relaxations. As suggested from the subtracted records in Fig. 6 *B*, these relaxations did not appear to contain a single exponential and were best described by two exponentials. Fig. 8 *A* shows a typical record for each isoform in which either a single exponential fit or the double fit procedure (see Materials and Methods) was applied to the complete relaxation. The difference between the original signal and the two fit procedures is also shown. The single exponential fit resulted in a significant error at times close to the voltage step, whereas the absence of any deviation in the difference signal for the double exponential fit confirmed that this was the preferable fitting function.

The voltage-dependence of the two time constants obtained from the fit procedure is shown in Fig. 8 *B*, pooled from the same oocytes as for the *Q-V* data. For each isoform, the faster time constant (τ_1) showed neither a systematic voltage-dependence nor dependence on pH_{ext}. Estimation of τ_1 was, however, hampered by the temporal resolution at times close to the voltage step afforded by the two-electrode voltage clamp, particularly for small voltage steps. However, the slower relaxation (τ_2), did show a clear "bell"-shaped voltage dependence. At $pH_{ext} = 6.2$ there was a significant shift in the maximum of the τ-*V* data toward depolarizing potentials, and the maximum τ also increased. For *flr* NaPi-IIb, the slower component was also strongly affected by pH_{ext}, particularly for $V > 0$ mV. For $V < 0$ mV, the low amplitude of this component made resolution difficult because of noise contamination, and we were unable to obtain consistent exponential fits in this region with the level of expression available ($I_p \approx -100$–200 nA at 1 mM P_i). Nevertheless, for $V > 0$ mV, the τ-*V* data for *flr* NaPi-IIb showed the same trend at depolarizing potentials. Moreover, although we could detect charge movement at $pH_{ext} = 5.6$, separation of the relaxations into two components was not possible due to the poor signal-to-noise ratio.

These findings indicated that in the absence of external substrates, changes in pH_{ext} altered the kinetics of charge movements associated with functional type II NaPi protein. Moreover, despite differences in relaxation kinetics, both isoforms showed the same qualitative dependence on pH_{ext} in 0 mM Na^+_{ext}. The τ-*V* data for the slow component were quantified by fitting Eq. 2 to the mean estimate of τ at each potential. The fitting results, summarized in Table 2, indicated that like the *Q-V* data, the apparent valency remained constant. Furthermore, these data suggested that the slow relaxation could be adequately described by a single transition Boltzmann model with one zero-voltage transition rate (k^o_{21}) that was pH-dependent for both isoforms.

DISCUSSION

We have studied the effect of protons on the steady-state and pre-steady-state kinetics of two members of the type II Na^+/P_i cotransporter family under voltage clamp conditions. Our aim was to identify proton-sensitive transitions that give rise to the characteristic inverse relation between luminal proton concentration and P_i uptake at the renal brush border membrane in vivo. Expression of Na^+/P_i cotransporters in *Xenopus* oocytes, as opposed to using renal proximal tubule cell lines, for example, allowed us to characterize the pH-dependency of a specific membrane protein under controlled conditions. Moreover, the absence of significant proton-dependent charge movements in response to voltage steps applied to noninjected oocytes indicated that contamination of the pre-steady-state relaxations from endogenous proteins was negligible.

TABLE 1 Fit parameters for the *Q-V* relation derived from a single transition Boltzmann model applied to pre-steady-state relaxations in 0 mM Na^+_{ext}

	rat NaPi-IIa				*flr* NaPi-IIb			
pH_{ext}	7.4	6.8	6.2	5.6	7.4	6.8	6.2	5.6
Q_{max}	1.0	1.0	0.9	0.7	1.0	1.1	1.0	0.9
(norm)		±0.1	±0.1	±0.2		±0.1	±0.1	±0.1
z	−0.49	−0.46	−0.41	−0.49	−0.34	−0.31	−0.31	−0.34
	±0.05	±0.11	±0.07		±0.03	±0.02	±0.02	
$\Delta V_{0.5}$ (mV)	0	+12	+44	+128	0	+68	+143	+241
		±4	±9	±19		±18	±23	±22

Results obtained by fitting Eq. 3 to *Q-V* for oocytes that expressed *rat* NaPi-IIa ($n = 3$) and *flr* NaPi-IIb ($n = 6$). $\Delta V_{0.5}$ is the change in $V_{0.5}$ relative to the value of $V_{0.5}$ predicted from the fit for each cell at $pH_{ext} = 7.4$. Q_{max} was normalized to the value predicted from the fit for each cell at $pH_{ext} = 7.4$. At $pH_{ext} = 5.6$, z was constrained in each fit to the value obtained at $pH_{ext} = 7.4$.

We used two NaPi-II isoforms, whose strong dependency on pH_{ext} in the steady state was first shown by tracer uptake studies (Magnanin et al., 1993; Werner et al., 1994) and later by electrophysiology (Busch et al., 1994; Forster et al., 1997a, b; 1998; 1999a). Both isoforms also have the same stoichiometry (Forster et al., 1999a), similar apparent affinities for P_i and Na^+ (Busch et al., 1994; Forster et al., 1997b; 1998; 1999a) and, as shown in the present study, the steady-state dependence on pH_{ext} was also similar. The pH_{ext}-dependence could not be attributed to P_i titration alone and, taken together, the comparable steady-state data for the two isoforms suggested common site(s) of interaction of protons on the type II NaPi protein. The inhibition reported here is most likely not attributable to a reduction in the number of cotransporters in the membrane, as the effect could be rapidly reversed (on a time scale of seconds) and has been observed in BBMVs (e.g., Amstutz et al., 1985), where the endocytotic machinery is not present.

In this study we have concentrated on the influence of external protons. We found that a significant reduction (up to 1 pH units) in pH_{int} did not affect activity in the *cis-trans* cotransport mode. This finding was in accord with the findings of Burckhardt et al. (1981) using BBMVs, but contrasted with other studies using the same preparation (Saktor and Cheng, 1981; Strévey et al., 1990), which reported simulated vesicular P_i uptake with an outwardly directed proton gradient. However, in one of these studies (Saktor and Cheng, 1981) there was no Na^+ gradient (100 mM on both sides), a condition that we were unable to reproduce in the intact oocyte. Both Amstutz et al. (1985) and Strévey et al. (1990) did report a small *trans* stimulation of P_i influx with an inward Na^+ gradient, but these authors eliminated transmembrane potential as a driving force, whereas our measurements were done at $V_h = -50$ mV. With the experimental conditions used in the present study, we are therefore unable to exclude internal acidification as a potential modulator of type II Na^+/P_i cotransport kinetics. However, the lack of an effect of acidification of the oocyte cytosol on the steady-state response at either $pH_{ext} = 7.4$ or 6.2 suggested that if internal protons interact with the protein, they do not influence transitions that define the kinetics of the inwardly directed cotransport mode. Furthermore, we also found no evidence that protons could substitute for Na^+ as a co-substrate, which contrasts with the behavior of the sodium-glucose cotransporter, SGLT-1 (Hirayama et al., 1994, 1997).

The experimental approach that we used to identify specific steps sensitive to extrinsic parameters such as voltage and pH was to limit the number of observable states and/or modes of operation of the cotransporter and examine the pH sensitivity under these restricted conditions. The interpretation of our findings is based on the kinetic model that describes type II Na^+/P_i cotransport, depicted in Fig. 9. This is an ordered, symmetrical scheme in which three modes of operation are identifiable from experimental observation: empty carrier mode, slippage mode, and cotransport mode (for more details, see Forster et al. (1998)). The kinetic parameters for substrate interactions on the *trans* side are not yet available for the NaPi-II system, because to date no studies have been performed that allow direct access to the oocyte cytosol. Nevertheless, simulations using this model under zero *trans* conditions have adequately predicted the main features of the experimentally observed steady-state and pre-steady-state behavior (Forster et al., 1998). Previous characterizations of the pre-steady-state kinetics have indicated that charge movements recorded from both *rat* NaPi-IIa (Forster et al., 1998) and *flr* NaPi-IIb (Forster et al., 1997a, b) are also sensitive to pH_{ext}. However, the role that the pH sensitivity of these transitions plays in determining the observed effects on the cotransport mode was not established. Furthermore, model simulations of the pre-steady-state kinetics of each isoform (Forster et al., 1997b, 1998) predict rate constants for the transitions associated with empty carrier ($1 \Leftrightarrow 8$) and first Na^+ binding step ($1 \Leftrightarrow 2$) that are significantly different. This might suggest that these transitions are not the major determinants of conserved steady-state kinetic parameters, such as pH sensitivity.

Cotransport mode in the steady-state

Both isoforms showed evidence of rate-limiting behavior at hyperpolarizing potentials, particularly for $pH_{ext} < 6.8$. It

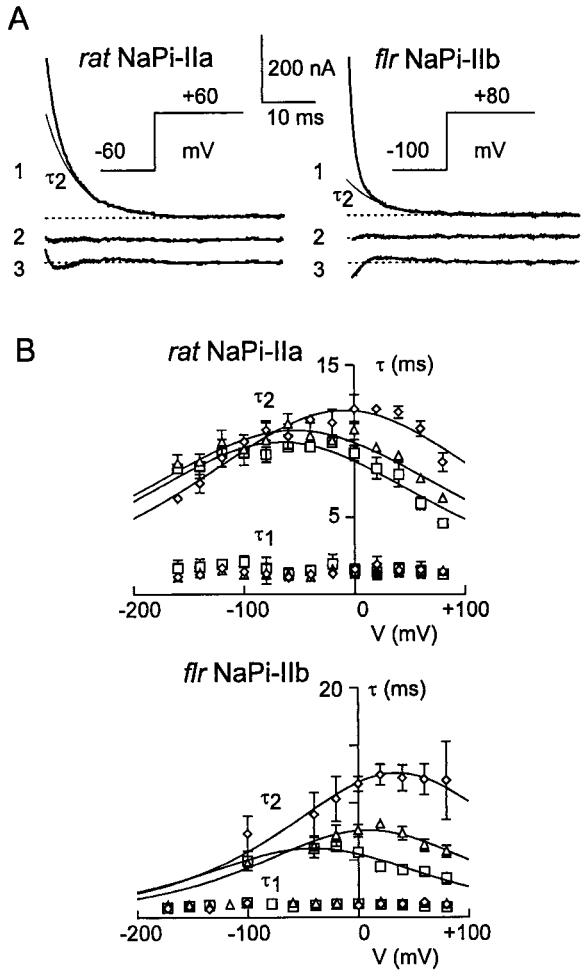

FIGURE 8 Voltage-dependent characteristics of relaxations in 0 mM Na^+. (*A*) Exponential curve fitting applied to pre-steady-state relaxations recorded in ND0 at pH_{ext} = 7.4, induced by voltage steps indicated. The response to ND0, pH_{ext} = 5.0, was subtracted to eliminate the endogenous components. *Trace 1*: data and slow fitted component (τ_2) superimposed (*rat* NaPi-IIa: τ_1 = 2.2 ms, τ_2 = 5.8 ms; *flr* NaPi-IIb: τ_1 = 1.2 ms, τ_2 = 6.3 ms). *Trace 2*: difference between double exponential fit (see Materials and Methods) and data. *Trace 3*: difference between a single exponential fit over the same time interval and data (*rat* NaPi-IIa: τ = 4.2 ms; *flr* NaPi-IIb: τ = 2.1 ms). The first 2 ms of the data traces were blanked during the charging period of the oocyte membrane. (*B*) Voltage-dependence of time constants (τ-*V*) obtained by fitting exponentials to the subtracted relaxation currents for pH_{ext} = 7.4 (□), 6.8 (△), and 6.2 (◇). The two exponential components are designated τ_1 and τ_2. Data were pooled from representative oocytes from the same batch, which expressed *rat* NaPi-IIa (n = 4) and *flr* NaPi-IIb (n = 6). Solid lines are fits using Eq. 2 to the slower relaxation (see Table 2 for fit parameters).

was striking that at pH_{ext} = 6.2, the voltage dependence of the P_i response was almost absent in the range of potentials tested ($-100 \leq V \leq +20$ mV). This behavior suggested that protons interact with voltage-dependent steps in the transport cycle so that the overall transport rate became less voltage-dependent as pH_{ext} decreased. The shape of the *I-V* data also indicated that I_p at the hyperpolarizing limit decreased with pH_{ext}. These data were obtained at 100 mM Na^+ with 1 mM total P_i, and a reduction in the divalent P_i available could not account for the decrease in rate-limiting current. Our data would, however, be consistent with a pH_{ext}-dependent decrease in apparent affinity for Na^+. For the mouse renal NaPi-IIa isoform, expressed in *Xenopus* oocytes, Hartmann et al. (1995) found that a decrease of pH_{ext} from 7.8 to 6.3 at 1 mM total P_i increased the apparent Na^+ affinity coefficient (K_m^{Na}) from ≈50 mM to ≈80 mM, with no significant change in the apparent V_{max}. A pH-dependent increase in K_m^{Na} was previously reported by Amstutz et al. (1985) using the BBMV preparation, whereby a significant V_{max} effect was also observed. According to the scheme of Fig. 9, an increase in K_m^{Na} could be explained mechanistically by protons competing for occupancy of the Na^+ binding sites: i.e., interaction with either or both steps 1 ⇒ 2 and 3 ⇒ 4. Based on an interpretation of the pre-steady-state data (see below), we favor the latter transition as being the most likely one for proton interactions that affect K_m^{Na}. Moreover, our previous simulations of the kinetic scheme for type II Na^+/P_i cotransporter (Forster et al., 1998) indicated that transition rate constants for the final Na^+ binding step have a strong effect on the apparent K_m^{Na}.

That step 3 ⇔ 4 is affected by protons is also consistent with our finding of a Hill coefficient <-1 for the steady-state inhibition curves (Fig. 1 *B*), whereby two protons would compete for occupancy of the binding site(s) normally accessed by two Na^+ ions. In another Na^+-coupled transport system, Matskevitch et al.(1998) have reported that the pH sensitivity of the *myo*-inositol transporter SMIT leads to a decrease in V_{max} and shift in the apparent K_m^{Na}. Moreover, they obtained a Hill coefficient for the H^+ dose-dependency of 1.8. This is consistent with the Na^+ binding Hill coefficient of 2 reported for this cotransporter protein (Hager et al., 1995) and also implicates an interaction of protons with the cooperative Na^+ binding step.

Slippage mode

For superfusion in 0 mM P_i and 100 mM Na^+_{ext}, the transporter operates in the slippage mode. Under these conditions, when endogenous effects were taken into account, we were unable to detect an effect of pH_{ext} on the slippage current. Moreover, the constancy of the reversal potential under these conditions suggested that at the concentrations used here, protons do not substitute for Na^+ in the slippage mode. One feature of the steady-state slippage mode experiments should also be noted. We consistently found that the reversal potential (E_r) was <0, which is not predicted by the Nernst relation if Na^+ is the only species involved and if we assume a Na^+_{int} value of ≈10–20 mM. Nevertheless, as reported by Forster et al. (1998), a Nernstian shift in E_r does occur when Na^+_{ext} is reduced at constant pH_{ext}, which strongly suggested that Na^+ is the transported ion. One possible explanation for this anomaly is that our zero *trans*

TABLE 2 Fit parameters for the τ-V relation derived from a single transition Boltzmann model applied to pre-steady-state relaxations in 0 mM Na^+_{ext}

	rat NaPi-IIa			*flr* NaPi-IIb		
pH_{ext}	7.4	6.8	6.2	7.4	6.8	6.2
k^o_{12} (s^{-1})	28 ± 4	31 ± 2	40 ± 2	55 ± 5	73 ± 5	58 ± 4
k^o_{21} (s^{-1})	87 ± 2	70 ± 3	43 ± 2	128 ± 7	60 ± 4	27 ± 2
z	−0.41 ± 0.04	−0.34 ± 0.03	−0.46 ± 0.03	−0.52 ± 0.05	−0.54 ± 0.05	−0.52

Parameters were obtained from fitting Eq. 2 to the mean of pooled data for the slower relaxation (τ_2) (see Fig. 8 *B*) for oocytes that expressed *rat* NaPi-IIa ($n = 4$) and *flr* NaPi-IIb ($n = 6$). Errors shown are SEM for the fit parameters. For fitting *flr* NaPi-IIb data at $pH_{ext} = 6.2$, z was constrained to the value predicted at $pH_{ext} = 7.4$.

assumption is invalid. Finite cytosolic Na^+ and P_i, the magnitude of which we have no direct control over in the intact oocyte, would theoretically contribute a steady-state outward current and thereby affect the thermodynamic equilibrium potential. Similar anomalous behavior of the slippage current was reported by Umbach et al. (1990) for the sodium glucose cotransporter, SGLT-1. Indeed, our simulations of the steady-state current (see below) predict a reversal potential of −20 mV when an internal P_i of only 0.1 mM is assumed.

Further insight into the pH_{ext}-dependent mechanism was obtained from pre-steady-state relaxations, whereby a significant shift in the steady-state charge distribution ($V_{0.5}$) and the maximum of the τ-V relationship were found, as previously reported for the *rat* NaPi-IIa (Forster et al., 1998) and *flr* NaPi-IIb (Forster et al., 1997a). Moreover, both Q_m and z, predicted from a single Boltzmann fit, remained essentially constant. This result also supported the notion that protons alter the kinetics of either the binding of the first Na^+ ion or the empty carrier, or both, without affecting the net charge movement. We have previously shown that reducing Na^+_{ext} at $pH_{ext} = 7.4$ leads to a shift in $V_{0.5}$ toward hyperpolarizing potentials for the Q-V curve and a concomitant shift in the maximum of the τ-V curve (Forster et al., 1997b, 1998). That we observed a shift in the opposite (depolarizing) direction as pH_{ext} was decreased suggested that protons neither compete for occupancy of the first Na^+ binding site nor block Na^+ access to this site, since the latter case would be equivalent to an apparent reduction in Na^+_{ext}.

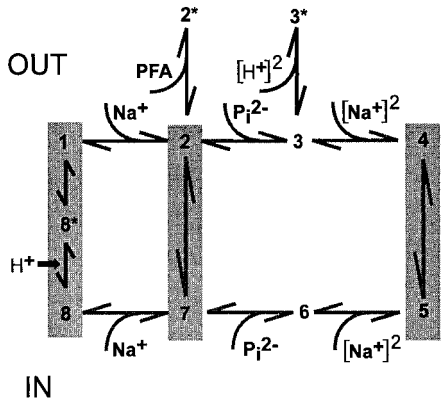

FIGURE 9 Kinetic scheme for type II Na^+/P_i cotransport. The transmembrane transitions that give rise to the three experimentally observed modes of operation (empty carrier: 1 ⇔ 8, slippage: 2 ⇔ 7, and cotransport 4 ⇔ 5) are indicated as boxed transitions. The final Na^+ binding, which involves two Na^+ ions, is lumped as a single transition. A proposed intermediate, empty carrier state (8*) accounts for the two exponential components detected in the empty carrier relaxations. PFA is assumed to place the system in an inhibited state 2* that prevents both slippage and cotransport modes. Two external protons compete with Na^+ for occupancy of state 4 by driving the system into an inhibited state 3*. Protons also interact with the backward transition of the empty carrier (8* ⇔ 8).

Empty carrier mode

The charge movements that remained when superfusing in ND0 were most likely also associated with functional NaPi-IIa/b protein. In the model of Fig. 9, these could be contributed by conformational changes of the empty carrier (1 ⇔ 8) and/or movement of internal Na^+ ions to the *trans* binding site (7 ⇔ 8). Although we cannot fully exclude potential contributions of the latter partial reaction, in the absence of experimental evidence to the contrary, we shall assume that the observed charge movement is entirely due to the empty carrier. We also note that Chen et al. (1996), using the cut-open oocyte technique, recorded charge movements from oocytes expressing SGLT-1 in the nominal absence of Na^+ on either side of the membrane.

We previously reported that a reduction in pH_{ext} appeared to suppress charge movements in 0 mM Na^+_{ext} for *rat* NaPi-IIa (Forster et al., 1998), but not for *flr* NaPi-IIb (Forster et al., 1997b). In the latter study, we only analyzed signals containing the full oocyte charging transient which, however could easily have masked more rapid pre-steady-state components. In the present study, to better resolve pH_{ext}-dependent changes in the pre-steady-state kinetics in 0 mM Na^+_{ext}, we subtracted the response at $pH_{ext} = 5.0$, under the assumption that any charge movements related to NaPi-II at this pH were negligible in the voltage range examined; i.e., at $pH_{ext} = 5.0$, charges are immobilized for $V < +100$ mV. The Q-V data for both isoforms, after adjustment to account for $Q(V_h)$ and normalization to Q_{max}, indicated that decreasing pH_{ext} induced a systematic shift in $V_{0.5}$, whereas both Q_{max} and z changed little with pH_{ext}. This suggested that protonation of the NaPi-II protein altered the voltage-de-

pendence of the empty carrier from the extracellular side by displacing the intrinsic charge distribution toward depolarizing potentials. This interpretation implies that even at $pH_{ext} = 5.0$, intrinsic charges can still be displaced if the membrane becomes sufficiently depolarized. The subtraction procedure may, however, result in an underestimation of Q for large depolarizing voltage steps that could account for the decrease in normalized Q_{max} seen at the lower pH_{ext}, particularly for *rat* NaPi-IIa.

Relaxations in ND0 were best described by two well-separated exponential components, one of which was strongly pH-dependent. The faster component had a τ close to that of the membrane charging ($\approx$1 ms). With the whole oocyte voltage clamp this was not easily resolvable and might arise from a measurement artifact or charge movements associated with endogenous protein. However, two lines of evidence do not support this explanation. First, the fast component was not observed in noninjected oocytes under the same superfusion conditions. Second, the estimated total charge movement (including both fast and slow components) in ND0 correlated with that measured in ND100. We have previously shown that this also correlates with P_i-induced electrogenic cotransport (Forster et al., 1997b, 1998), and this correlation has also been shown to hold in the case of other Na^+-coupled cotransporters (e.g., Loo et al., 1993; Wadiche et al., 1995). It is interesting to note that for the Na^+-coupled glucose cotransporter (SGLT1), Chen et al. (1996), by using the higher resolution cut-open oocyte technique, also detected a second, faster relaxation component that was attributed to the empty carrier.

Both isoforms showed qualitatively similar changes to the Q-V curves and the τ-V curve of the slow relaxation with pH_{ext}, despite obvious differences in the absolute kinetics of this component between isoforms. These differences in the empty carrier kinetics would most likely account for the different kinetics we have previously reported for pre-steady-state relaxations recorded in normal extracellular Na^+ ($\approx$100 mM) (Forster et al., 1997b, 1998). Under the assumption that the empty carrier relaxations arise from a sequential charge translocation process, our finding of two non-zero τ values indicated that this mode should be described, at minimum, by a three-state system. Therefore, we modified our previous model (Forster et al., 1997, 1998) to include an additional intermediate state (8*) (see scheme of Fig. 9). From both the τ-V and Q-V analyses an apparent valency, $z \approx -0.4$, could be assigned to the slow component. In this respect we would expect the estimate of z from Q-V data to be in error. These data were obtained integrating the total charge movement, but were fit on the basis of a single Boltzmann function, and z would most likely represent a weighted average from both components (see also Chen et al. (1996)). The limited temporal resolution of the two-electrode voltage clamp, together with the relatively low expression levels we obtained with both isoforms, meant that a complete characterization of the fast component was not possible.

Modeling pH_{ext} interactions with NaPi-II

To test the validity of our interpretations with respect to the overall kinetic scheme of Fig. 9, we simulated the pH_{ext}-dependence of the pre-steady-state and steady-state behavior of a single transport molecule. To model the competitive interaction of protons with the final Na^+ binding step, we included a transition to an inhibited state (3*), whereby two protons substitute for the two Na^+ ions and the occupancy of state 4 was thereby inhibited. The rate constant for the transition $3 \Rightarrow 3^*$ was chosen to take account of the apparent $K_i \approx 0.4$ μM derived from the steady-state inhibition data. For the empty carrier, the pH_{ext} dependence of the single Boltzmann τ-V fit to the slow component indicated that the apparent backward rate constant at 0 mV was sensitive to pH_{ext} (see Table 2). A sequential kinetic scheme for the empty carrier transitions that can account for this dependency (see Fig. 9) and give the observed separation of the two relaxation components comprises a slow pH-dependent backward transition and a fast pH-independent transition. In this scheme, the backward rate constant k^o_{8*8} was scaled according to the predictions from fitting Eq. 2 to the slow component τ-V data (Table 2). For the purpose of illustrating the pH-dependent effects, we used the voltage-dependent parameters derived from the *flr* NaPi-IIb data. Substitution of *rat* NaPi-IIa voltage-dependent parameters gave qualitatively similar results. The parameters for the other substrate-dependent transitions were chosen to give reasonable predictions for the steady-state behavior (apparent $K^{Pi}_m \approx 0.1$ mM; apparent $K^{Na}_m \approx 50$ mM). For all simulations we assumed a saturating external $P_i = 3$ mM.

Fig. 10 *A* shows simulated pre-steady-state relaxations for a voltage step from -100 mV to $+60$ mV at the two pH_{ext} values. In 0 mM Na^+_{ext}, the two components of the empty carrier charge movement are readily apparent at $pH_{ext} = 6.2$. In 100 mM Na^+_{ext}, the predicted relaxation (at $pH_{ext} = 7.4$) also includes charge movement from the unbinding of Na^+ and appears as a single component relaxation as observed in practice (compare with Fig. 5 *B*). Although we could only detect one relaxation by exponential curve-fitting the measured data, our description of the Q-V data as a single Boltzmann function (Fig. 5 *D*) is a simplification. This is also true in the case of the empty carrier where the charge movement comprises two transitions. Fig. 10, *B* and C show the corresponding τ-V curves and Q-V curves for the empty carrier at $pH_{ext} = 7.4$ and 6.2, respectively, and confirm the shift in voltage-dependence observed for the slower component (τ_2).

In the steady state, the simulated I-V curves for the slippage mode alone (Fig. 10 *D*, *top*) predicted only marginal changes in the slippage current with pH. The reversal potential at -20 mV arises from having a finite internal P_i

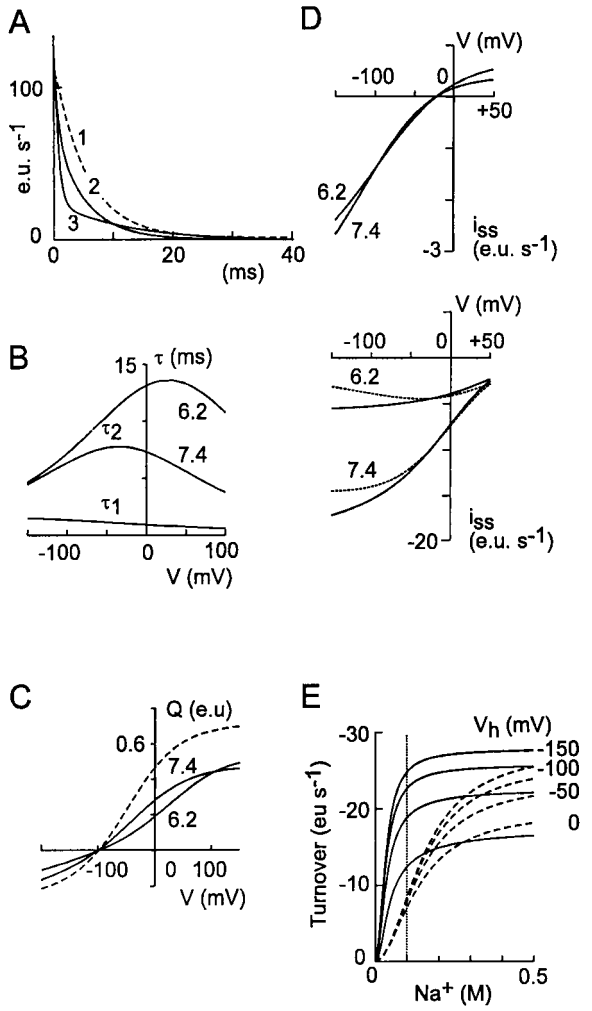

FIGURE 10 Simulations of the effect of pH_{ext} on the pre-steady-state and steady-state kinetics. Rate constants and other parameters were assigned to the transitions between states of the kinetic scheme of Fig. 9 for $pH_{ext} = 7.4$, as follows: $k^o_{12} = 10000\ M^{-1}\ s^{-1}$; $k^o_{21} = 500\ s^{-1}$; $k^o_{23} = 1000\ mM^{-1}\ s^{-1}$; $k^o_{32} = 100\ s^{-1}$; $k^o_{34} = 100000\ M^{-2}\ s^{-1}$; $k^o_{43} = 100\ s^{-1}$; $k^o_{45} = 25\ s^{-1}$; $k^o_{54} = 25\ s^{-1}$; $k^o_{27} = 2.5\ s^{-1}$; $k^o_{18*} = 1000\ s^{-1}$; $k^o_{8*1} = 100\ s^{-1}$; k^o_{8*8} ($pH_{ext} = 7.4$) $= 100\ s^{-1}$; k^o_{8*8} ($pH_{ext} = 6.2$) $= 30\ s^{-1}$; $k^o_{88*} = 50\ s^{-1}$, $k^o_{33*} = 6250\ \mu M^{-2}\ s^{-1}$; $k^o_{3*3} = 100\ s^{-1}$; $k^o_{56} = 100\ s^{-1}$; $k^o_{65} = 100000\ M^{-2}\ s^{-1}$; $k^o_{67} = 1000\ s^{-1}$; $k^o_{78} = 1000\ s^{-1}$; $k^o_{87} = 2000\ M^{-1}\ s^{-1}$; z_{12} ($= -1.\alpha'$) $= -0.25$; z_{8*1} ($= -1.\delta''$) $= -0.25$; z_{88*} ($= -1.\delta'$) $= -0.5$; z_{87} ($= -1.\alpha''$) $= 0$. For simulations the temperature was taken as 20°C; internal $Na^+ = 10$ mM and internal $P_i = 0.1$ mM. Rate constants were not assigned to the transition to the PFA bound state ($2 \Leftrightarrow 2^*$). Rate constants k_{72}, k^o_{76} were constrained by the conditions for microscopic reversibility (see Appendix). (*A*) Simulated pre-steady-state relaxations induced by a voltage step from −100 mV to +60 mV. *Trace 1:* 100 mM Na^+_{ext}, $pH_{ext} = 7.4$; *trace 2:* 0 mM Na^+_{ext}, $pH_{ext} = 7.4$; *trace 3:* 0 mM Na^+_{ext}, $pH_{ext} = 6.2$. (*B*) Simulation of the voltage-dependence of τ values for the relaxations associated with the empty carrier at pH_{ext} indicated. Only τ_2 is affected by pH. (*C*) Steady-state charge distribution as a function of voltage (*Q-V*) predicted from Eq. A1 for the same pH_{ext} as in (*A*) and (*B*) in 0 mM Na^+_{ext} (*solid lines*). The dashed line is the steady-state charge distribution with 100 mM Na^+_{ext}. (*D*) Effect of pH_{ext} on steady-state current-voltage (*I-V*) for slippage mode (*top*) and cotransport mode (*bottom*). Steady-state current i_{ss} is the equivalent current per transporter, given by Eq. A2. For these simulations, external $P_i = 3$ mM, external $Na^+ = 100$ mM, internal $Na^+ = 10$ mM, and internal $P_i = 0.1$ mM. Dotted traces in cotransport mode *I-V* simulation represent net current/cotransporter after subtraction of slippage component. (*E*) Na^+ activation curves predicted for $pH_{ext} = 7.4$ (*solid lines*) and $pH_{ext} = 6.2$ (*dashed lines*) $V_h = -150$, −100, −50, and 0 mV. The apparent K^{Na}_m values (in mM) at $pH_{ext} = 7.4$ (6.2) were −150 mV: 38 (153); −100 mV: 41 (153); −50 mV: 50 (150); 0 mV: 75 (135). Vertical line indicates $Na^+_{ext} = 100$ mM.

(= 0.1 mM) in the simulations. In contrast, cotransport mode steady-state current is strongly pH-dependent (Fig. 10 *D*, *bottom*). This results from the combined effects of changing the rate constant k^o_{8*8} and competitive inhibition of the last Na^+ binding step, which alter the voltage-dependence and transport rate at hyperpolarizing potentials, respectively. Because in practice the response in the control solution was implicitly subtracted from the P_i-induced response to eliminate oocyte endogenous currents, the slippage current would also be subtracted from the P_i-induced current. The slippage-adjusted *I-V* curves are also shown (*dotted lines*) and at $pH_{ext} = 6.2$, which indicate an upward inflexion at hyperpolarizing potentials, in qualitative agreement with the measured *I-V* data.

Finally, Fig. 10 *E* shows the simulated steady-state Na^+ activation curves for the two nominal pH_{ext} values and four holding potentials (V_h). The simulations predict that a significant increase in the apparent Na^+ affinity constant (K^{Na}_m) occurs at the lower pH_{ext}, which is in agreement with the BBMV study of Amstutz et al. (1985) and the oocyte study of Hartmann et al. (1995). Moreover, at 100 mM Na^+_{ext}, the transport rate is relatively insensitive to V_h at $pH_{ext} = 6.2$ compared with $pH_{ext} = 7.4$, as observed (see Fig. 2 *B*). In contrast, at saturating Na^+_{ext} there is a V_{max} dependence on V_h for each pH_{ext}, which indicates that under these conditions voltage-dependent transitions are rate-limiting.

CONCLUSIONS

This study identifies two transitions in the type II NaPi cotransport cycle that are modulated by external protons. First, protons interact with the empty carrier by altering a rate constant associated with the empty carrier *cis-trans* conformational change. This shifts the steady-state charge distribution of the empty carrier toward depolarizing potenials and can account for the loss of voltage-dependency for $V < 0$. Second, protons compete with Na^+ ions at the last Na^+ binding step before translocation of the fully loaded protein, which increases the apparent K^{Na}_m. Despite differences in the pre-steady-state voltage-dependent kinetics of the two NaPi-II isoforms that we have previously reported, the similarity of their behavior with respect to changes in external pH suggests that there are common sites of interaction of protons with the protein.

APPENDIX

Simulating the kinetics of the type II Na^+/P_i cotransporter

The formulation of the rate equations describing the transitions was similar to that described in detail by Parent et al. (1992) for the sodium-glucose cotransporter SGLT-1. Non-rapid equilibrium conditions were assumed. Rate constants for transitions that involve charge movement (first Na^+ binding/unbinding and empty carrier, see Fig. 8) were expressed in terms of the Eyring-Boltzmann formulation by assuming symmetrical energy barriers. For a given transmembrane voltage V, the rate constants for a transition between states i and j that involve charge movement (apparent valency z_{ij}) were expressed as $k_{ij} = k^o_{ij} \exp(z_{ij}eV/2kT)$ and $k_{ji} = k^o_{ji} \exp(-z_{ij}eV/2kT)$, where e, k, and T have their usual meanings and k^o_{ij}, k^o_{ji} are the transition rates at $V = 0$. For transitions involving ligand binding, the binding/unbinding rates were expressed as: $k_{ij} = [S]^n k^o_{ij}$ and $k_{ji} = k^o_{ji}$, respectively, where [S] is the substrate concentration and n is the order of the binding reaction. For example, the final Na^+ binding step ($3 \Leftrightarrow 4$) and the proton interaction with this step ($3 \Leftrightarrow 3^*$), were modeled as a single transitions with $n = 2$.

An alternating access-type cotransport mechanism was assumed (e.g., Läuger, 1991) in which the charge of the empty carrier ($= -1$), moves between the *cis* and *trans* conformations through an equivalent electrical distance δ and thereby exposes the binding site for a single Na^+ ion at the respective interface. To account for the two components in the empty carrier pre-steady-state relaxations, $\delta = \delta'' + \delta''$, where $\delta'$and δ'' are the equivalent electrical distances associated with transitions $8 \Leftrightarrow 8^*$ and $8^* \Leftrightarrow 1$, respectively. The Na^+ ion reaches its binding site by moving through equivalent electrical distances α' and α'', from the *cis* and *trans* membrane-solution interfaces, respectively, so that $\alpha' + \alpha'' + \delta = 1$.

To preserve microscopic reversibility, rate constants k_{72} and k^o_{76} were defined by:

$$k_{72} = \frac{k^o_{12}k_{27}k^o_{78}k^o_{88*}k^o_{8*1}}{(k^o_{21}k^o_{18*}k^o_{8*8}k^o_{87})}$$

and

$$k^o_{76} = \frac{k_{67}k_{72}k^o_{23}k_{34}k_{45}k_{56}}{(k_{65}k_{54}k_{43}k_{32}k_{27})}.$$

The differential equations describing the state transitions were solved for the state occupancies and eigenvalues by using matrix methods (Forster et al., 1998). The eigenvalues gave the time constants for the components of the pre-steady-state relaxations. The state occupancies (X_i), together with the apparent valencies (z_{ij}), were used to obtain the steady-state charge distribution. For a translocation of one net charge through the transmembrane field, at any holding potential V_h, the charge movement/cotransporter $Q(V - V_h)$, evoked by a voltage step to V can be expressed as:

$$\begin{aligned} Q(V - V_h) &= 1 \cdot [\alpha''(\Delta X_8) + (\alpha'' + \delta'')(\Delta X_{8*}) \\ &\quad + (\alpha'' + \delta'' + \delta')(\Delta X_1) + (\alpha'' + \delta'' + \delta' + \alpha')(\Delta X_2)] \\ &= \alpha''(\Delta X_8) + (\alpha'' + \delta'')(\Delta X_{8*}) \\ &\quad + (\alpha'' + \delta)(\Delta X_1) + \Delta X_2 \end{aligned} \quad \text{(A1)}$$

where ΔX_i is the change in occupancy of state i.

The empty carrier transition ($8 \Leftrightarrow 1$) is the only transmembrane transition that involves a net charge transfer, therefore the transmembrane current per transporter (i_{ss}) is given by:

$$i_{ss} = -1 \cdot (X_{8*}k_{8*8} - X_8k_{88*} + X_1k_{18} - X_{8*}k_{8*1}) \quad \text{(A2)}$$

This work was supported by grants to H.M. from the Swiss National Science Foundation (SNF 31-46523), the Hartmann Müller-Stiftung (Zurich), the Olgar Mayenfisch-Stiftung (Zurich), and the Schweizerischer Bankgesellschaft (Zurich) (Bu704/7-1).

REFERENCES

Amstutz, M., M. Mohrmann, P. Gmaj, and H. Murer. 1985. Effect of pH on phosphate transport in rat renal brush border vesicles. *Am. J. Physiol. Renal Physiol.* 248:F705–F710.

Axon Instruments. 1999. pClamp User's Guide. Axon Instruments Inc., Foster City, CA. 217–236.

Bindels, R. J. M., L. A. M. van den Broek, and C. H. van Os. 1987. Effect of pH on the kinetics of Na^+-dependent phosphate transport in rat renal brush-border membranes. *Biochim. Biophys. Acta.* 897:83–92.

Burckhardt, G., H. Stern, and H. Murer. 1981. The influence of pH on phosphate transport into rat renal brush border membrane vesicles. *Pflügers Arch.* 390:191–197.

Busch, A. E., S. Waldegger, T. Herzer, J. Biber, D. Markovich, G. Hayes, H. Murer, and F. Lang. 1994. Electrophysiological analysis of Na^+/P_i cotransport mediated by a transporter cloned from rat kidney in Xenopus oocytes. *Proc. Natl. Acad. Sci. U.S.A.* 91:8205–8208.

Chen, X. Z., M. J. Coady, and J.-Y. Lapointe. 1996. Fast voltage clamp discloses a new component of pre-steady-state currents from the Na^+-glucose cotransporter. *Biophys. J.* 71:2544–2552.

Cheng, L., and B. Sacktor. 1981. Sodium gradient-dependent phosphate transport in renal brush border membrane vesicles. *J. Biol. Chem.* 256:1556–1564.

Choe, H., H. Zhou, L. G. Palmer, and H. Sackin. 1997. A conserved cytoplasmic region of ROMK modulates pH sensitivity, conductance and gating. *Am. J. Physiol. Renal Physiol.* 273:F516–F529.

Forster, I., J. Biber, and H. Murer. 1997a. Modulation of the voltage-dependent kinetics of renal type II Na^+/P_i cotransporters by external pH. *J. Am. Soc. Nephrol.* 8:2611*a*. (Abstr.).

Forster, I. C., and N. G. Greeff. 1992. The early phase of sodium channel gating current in the squid giant axon. *Eur. Biophys. J.* 21:99–116.

Forster, I., N. Hernando, J. Biber, and H. Murer. 1998. The voltage dependence of a cloned mammalian renal type II Na^+/P_i cotransporter (NaPi-2). *J. Gen. Physiol.* 112:1–18.

Forster, I., D. D. F. Loo, and S. Eskandari. 1999a. Stoichiometry and Na^+ binding cooperativity of rat and flounder renal type II Na^+-P_i cotransporters. *Am. J. Physiol. Renal Physiol.* 276:F644–F649.

Forster, I., M. Traebert, M. Jankowski, G. Stange, J. Biber, and H. Murer. 1999b. Protein kinase C activators induce membrane retrieval of type II Na-phosphate cotransporters expressed in Xenopus oocytes. *J. Physiol. (Camb.).* 517:2:327–340.

Forster, I. C., C. A. Wagner, A. E. Busch, F. Lang, J. Biber, N. Hernando, H. Murer, and A. Werner. 1997b. Electrophysiological characterization of the flounder type II Na^+/P_i cotransporter (NaPi-5) expressed in *Xenopus laevis* oocytes. *J. Membr. Biol.* 160:9–25.

Gottschalk, C. W., W. E. Lassiter, and M. Mylle. 1960. Localization of urine acidification in the mammalian kidney. *Am. J. Physiol.* 198: 581–585.

Hager, K., A. Hazama, H. M. Kwon, D. D. F. Loo, J. S. Handler, and E. M. Wright. 1995. Kinetics and specificity of the renal Na^+/*myo*-inositol cotransporter expressed Xenopus oocytes. *J. Membr. Biol.* 143:103–113.

Hartmann, C. M., C. A. Wagner, A. E. Busch, D. Markovich, J. Biber, F. Lang, and H. Murer. 1995. Transport characteristics of a murine renal Na/Pi-cotransporter. *Pflügers Arch.* 430:830–836.

Hilfiker, H., O. Hattenhauer, M. Traebert, I. Forster, H. Murer, and J. Biber. 1998. Characterization of a murine type II sodium-phosphate cotransporter expressed in mammalian small intestine. *Proc. Natl. Acad. Sci. U.S.A.* 95:14564–14569.

Hirayama, B., D. D. F. Loo, and E. M. Wright. 1994. Protons drive sugar transport through the Na^+/glucose cotransporter (SGLT1). *J. Biol. Chem.* 269:21407–21410.

Hirayama, B., D. D. F. Loo, and E. M. Wright. 1997. Cation effects on protein conformation and transport in the Na^+/glucose cotransporter. *J. Biol. Chem.* 272:2110–2115.

Knox, F. G., and A. Haramati. 1985. Renal regulation of phosphate excretion. *In* The Kidney: Physiology and Pathophysiology, 2nd Ed. D. W. Seldin and G. Giebisch, editors. Raven Press, New York. 1381–1396.

Kohl, B., P. Herter, B. Huelseweh, M. Elger, H. Hentschel, R. H. Kinne, and A. Werner. 1996. Na-P_i cotransport in flounder: same transport system in kidney and intestine. *Am. J. Physiol.* 270:937–944.

Läuger, P. 1991. Electrogenic Ion Pumps. Sinauer Assoc. Inc., Sunderland, MA. 74–77.

Loo, D. F., A. Hazama, S. Supplisson, E. Turk, and E. M. Wright. 1993. Relaxation kinetics of the Na^+/glucose cotransporter. *Proc. Natl. Acad. Sci. U.S.A.* 90:5767–5771.

Magnanin, S., A. Werner, D. Markovich, V. Sorribas, G. Stange, J. Biber, and H. Murer. 1993. Expression cloning of human and rat renal cortex Na/P_i cotransport. *Proc. Natl. Acad. Sci. U.S.A.* 90:5979–5983.

Matskevitch, J., C. A. Wagner, T. Risler, H. M. Kwon, J. S. Handler, S. Waldegger, A. E. Busch, and F. Lang. 1998. Effect of extracellular pH on the *myo*-inositol transporter SMIT expressed in *Xenopus* oocytes. *Pflügers Arch.* 436:854–857.

Murer, H., and J. Biber. 1992. Renal tubular phosphate transport. Cellular mechanisms. *In* The Kidney: Physiology and Pathophysiology, 2nd Ed. D. W. Seldin and G. Giebisch, editors. Raven Press, New York. 2481–2509.

Murer, H., and J. Biber. 1996. Molecular mechanisms of renal apical Na phosphate cotransport. *Annu. Rev. Physiol.* 58:607–618.

Murer, H., N. Hernando, I. Forster, and J. Biber. 2000. Proximal tubular phosphate reabsorption: molecular mechanisms. *Physiol. Rev.* In press.

Parent, L., S. Supplisson, D. D. F. Loo, and E. M. Wright. 1992. Electrogenic properties of the cloned Na^+/Glucose cotransporter. II. A transport model under nonrapid equilibrium conditions. *J. Membr. Biol.* 125: 63–79.

Quamme, G. A., and N. M. L. Wong. 1984. Phosphate transport in the proximal convoluted tubule: effect of intraluminal pH. *Am. J. Physiol. Renal Physiol.* 246:F323–F333.

Saktor, B., and L. Cheng. 1981. Sodium gradient-dependent phosphate transport in renal brush border membrane vesicles. *J. Biol. Chem.* 256:8080–8084.

Samarzija, I., V. Molnar, and E. Frömter. 1982. pH-dependence of phosphate in rat renal proximal tubule. *Proc. European Dialysis Transplant Assoc.* 19:779–783.

Strévey, J., S. Giroux, and R. Béliveau. 1990. pH gradient as an additional driving force in the renal re-absorption of phosphate. *Biochem. J.* 271: 687–692.

Umbach, J. A., M. J. Coady, and E. M. Wright. 1990. Intestinal Na^+/glucose cotransporter expressed in *Xenopus* oocytes is electrogenic. *Biophys. J.* 57:1217–1224.

Wadiche, J. I., J. L. Arriza, S. G. Amara, and M. P. Kavanaugh. 1995. Kinetics of a human glutamate transporter. *Neuron.* 14:1019–1027.

Werner, A., H. Murer, and R. K. H. Kinne. 1994. Cloning and expression of a renal Na-P_i cotransport system from flounder. *Am. J. Physiol. Renal Physiol.* 267:F311–F317.

Woodward, R. M., and R. Miledi. 1992. Sensitivity of Xenopus oocytes to changes in extracellular pH: possible relevance to proposed expression of atypical mammalian $GABA_B$ receptors. *Mol. Brain Res.* 16:204–210.